Variability of biomass burning aerosol optical characteristics in southern Africa during the SAFARI 2000 dry season campaign and a comparison of single scattering albedo estimates from radiometric measurements

T. F. Eck,[1,2] B. N. Holben,[2] D. E. Ward,[3] M. M. Mukelabai,[4] O. Dubovik,[1,2] A. Smirnov,[1,2] J. S. Schafer,[2,5] N. C. Hsu,[1] S. J. Piketh,[6] A. Queface,[6] J. Le Roux,[7] R. J. Swap,[8] and I. Slutsker[2,5]

[1] Measurements of the column-integrated aerosol optical properties in the southern African region were made by Aerosol Robotic Network (AERONET) Sun-sky radiometers at several sites in August–September 2000 as a part of the Southern African Regional Science Initiative (SAFARI) 2000 dry season field campaign. Fine mode biomass burning aerosols dominated in the northern part of the study region (Zambia), which is an active burning region, and other aerosols including fossil fuel burning, industrial, and aeolian coarse mode types also contributed to the aerosol mixture in other regions (South Africa and Mozambique), which were not as strongly dominated by local burning. The large amount of smoke produced in the north lead to a north-south gradient in aerosol optical depth (τ_a) in September, with biomass burning aerosol concentrations reduced by dispersion and deposition during transport. Large average diurnal variations of τ_a (typical diurnal range of 25%) were observed at all sites in Zambia as a result of large diurnal trends in fire counts in that region that peak in midafternoon. However, for all sites located downwind to the south, there was relatively little (~5–10%) average diurnal trend observed as the aerosol transport is not strongly influenced by diurnal cycles. AERONET radiometer retrievals of aerosol single scattering albedo (ω_0) in Zambia showed relatively constant values as a function of τ_a for τ_{a440} ranging from 0.4 to ~2.5. The wavelength dependence of ω_0 varied significantly over the region, with greater decreases for increasing wavelength at smoke-dominated sites than for sites influenced by a significant coarse mode aerosol component. Retrievals of midvisible ω_0 based on the fitting of Photosynthetically Active Radiation (PAR; 400–700 nm) flux measurements to modeled fluxes for smoke in Mongu, Zambia yielded an average value of 0.84. This is in close agreement with the estimated average of 0.85 derived from interpolation of the AERONET retrievals made at 440 and 675 nm for August–September 2000. The spectral dependence of ω_0 independently retrieved with the AERONET measurements and with diffuse fraction measurements in Mongu, Zambia was similar for both techniques, as a result of both methods retrieving the imaginary index of refraction (~0.030–0.035 on one day) with very little wavelength dependence. *INDEX TERMS:* 0305 Atmospheric Composition and Structure: Aerosols and particles (0345, 4801); 0360 Atmospheric Composition and Structure: Transmission and scattering of radiation; 0345 Atmospheric Composition and Structure: Pollution—urban and regional (0305); 3360 Meteorology and Atmospheric Dynamics: Remote sensing; 3359 Meteorology and Atmospheric Dynamics: Radiative processes; *KEYWORDS:* atmospheric aerosols, biomass burning, Africa, optical characteristics

[1]Goddard Earth Sciences and Technology Center, University of Maryland-Baltimore County, Baltimore, Maryland, USA.

[2]Biospheric Sciences Branch, National Aeronautics and Space Administration/Goddard Space Flight Center, Greenbelt, Maryland, USA.

[3]Enviropyronics, White Salmon, Washington, USA.

[4]Zambian Meteorological Department, Mongu, Zambia.

[5]Science Systems and Applications Inc., National Aeronautics and Space Administration/Goddard Space Flight Center, Greenbelt, Maryland, USA.

[6]Climatology Research Group, University of Witwatersrand, Gauteng, South Africa.

[7]Etosha Ecological Institute, Okaukuejo, Namibia.

[8]Department of Environmental Sciences, University of Virginia, Charlottesville, Virginia, USA.

1. Introduction

[2] Recent studies have emphasized the global significance of black carbon in atmospheric aerosols in relation to their influence on climate forcing [*Hansen et al.*, 2000; *Houghton et al.*, 2001]. *Jacobson* [2001] simulated large positive direct radiative forcings from black carbon in aerosols produced from fossil fuel and biomass combustion. For a mostly internal mixture of black carbon he suggests that the warming effect (through absorption) from black carbon aerosol direct forcing may almost balance the direct cooling effect (by scattering) of other anthropogenic aerosol species. In addition to direct effects for climate forcing, absorption of solar radiation by aerosols containing black carbon may also result in reduction of cloud cover by modification of the atmospheric temperature profile and evaporating clouds [*Hansen et al.*, 1997; *Ackerman et al.*, 2000].

[3] *Haywood and Ramaswamy* [1998] determined that the global direct radiative forcing of both biomass and fossil fuel black carbon were of nearly equal magnitude. The IPCC Third Assessment Report [*Houghton et al.*, 2001] suggests that source strengths for black carbon are nearly equal for fossil fuel and biomass burning on the global scale. However, they also state that the vast majority of fossil fuel burning occurs in the northern hemisphere, while biomass burning black carbon production is nearly evenly divided between the northern and southern hemispheres. Therefore biomass burning is by far the largest source of aerosol black carbon in the Southern Hemisphere. The majority of the biomass burning in the Southern Hemisphere occurs in the tropics in the dry season months of July–November [*Dwyer et al.*, 1998; *Holben et al.*, 2001].

[4] Recent studies of the optical characteristics of biomass burning aerosol types [*Dubovik et al.*, 2002; *Eck et al.*, 2001] have shown that the southern African savanna smoke is the most absorbing of all other major biomass burning regions investigated, which included Amazonian forest regions, South American cerrado (savanna) regions, and boreal forest regions. This is consistent with the findings of *Ward et al.* [1992, 1996] on the characteristics of burning from savanna fires in Africa and deforestation fires in Brazil. They found a much higher fraction of the biomass is consumed by flaming combustion in savanna ecosystems (∼85%) than for deforestation fires (50% or less). Since for flaming combustion, as much as 15–20% of the aerosol produced was black carbon compared to less than 3% for smoldering [*Ward et al.*, 1992, 1996], the phase of combustion is a major factor in determining the smoke absorption characteristics in different regions.

[5] In this paper we will focus on the optical characteristics of atmospheric aerosols in the southern African savanna region during the time period of the Southern African Regional Science Initiative (SAFARI) 2000 dry season field campaign, August–September 2000 [*Swap et al.*, 2002]. This time period is the peak of the dry season biomass burning activity and therefore biomass burning aerosols dominate other aerosol types at most of the sites investigated. Our analysis focuses on the data obtained from 10 Sun-sky radiometers distributed throughout southern Africa, which were a part of the Aerosol Robotic Network (AERONET [*Holben et al.*, 1998]). We present analyses of the spatial and temporal variability of aerosol optical depth (τ_a), its spectral dependence as parameterized by the Angstrom exponent (α), the dynamics of the retrieved aerosol size distributions, and investigate spectral absorption as parameterized by the single scattering albedo (ω_0).

2. Study Region, Instrumentation, and Methodology

2.1. Region of Study

[6] A map showing the locations of the AERONET Sun-sky radiometers utilized in this study, in addition to regional industrial centers is shown in Figure 1. Seven sites were located within the western half of Zambia in August–September 2000 in order to more completely characterize the biomass burning aerosols in this region of extensive savanna burning. Other AERONET sites which are analyzed in this study are located in Etosha Pan National Park, Namibia, Inhaca Island, Mozambique, Skukuza (in Kruger National Park), South Africa, and Bethlehem, South Africa. Several other AERONET sites operated for shorter duration time periods (∼1–2 weeks) and are not included in this analysis. The time period of the SAFARI 2000 dry season experiment, August through September, coincides with the peak periods of agricultural burning and thus the highest levels of τ_a for biomass burning aerosols. Subsidence from anticyclonic circulation is a dominant meteorological feature during much of the biomass burning season in this region with 4 stable vertical layers identified in the troposphere [*Garstang et al.*, 1996]. Altitudinal layering of aerosols associated with temperature inversions was observed with a micropulse lidar at a site in South Africa during SAFARI 2000 [*Campbell et al.*, this issue]. This atmospheric stability often results in cloudless or nearly cloudless sky conditions for extended periods at this time of the year.

2.2. Instrumentation

[7] All of the CIMEL Electronique CE-318 Sun-sky radiometer measurements reported in this paper were made with instruments that are a part of the AERONET global network. These instruments are described in detail by *Holben et al.* [1998], however a brief description will be given here. The automatic tracking Sun and sky scanning radiometers made direct Sun measurements with a 1.2° full field of view every 15 min at 340, 380, 440, 500, 675, 870, 940, and 1020 nm (nominal wavelengths). The direct Sun measurements take ∼8 s to scan all 8 wavelengths, with a motor driven filter wheel positioning each filter in front of the detector. These solar extinction measurements are then used to compute aerosol optical depth at each wavelength except for the 940 nm channel, which is used to retrieve total precipitable water in centimeters. The filters utilized in these instruments were ion assisted deposition interference filters with bandpass (full width at half maximum) of 10 nm except for the 340 nm channel at 2 nm and the 380 nm filter at 4 nm. Calibration of field instruments was performed by a transfer of calibration from reference instruments which were calibrated by the Langley plot technique at Mauna Loa Observatory (MLO), Hawaii. The inter-calibration of field instruments was performed both pre- and post deployment at Goddard Space Flight Center (GSFC) and a linear
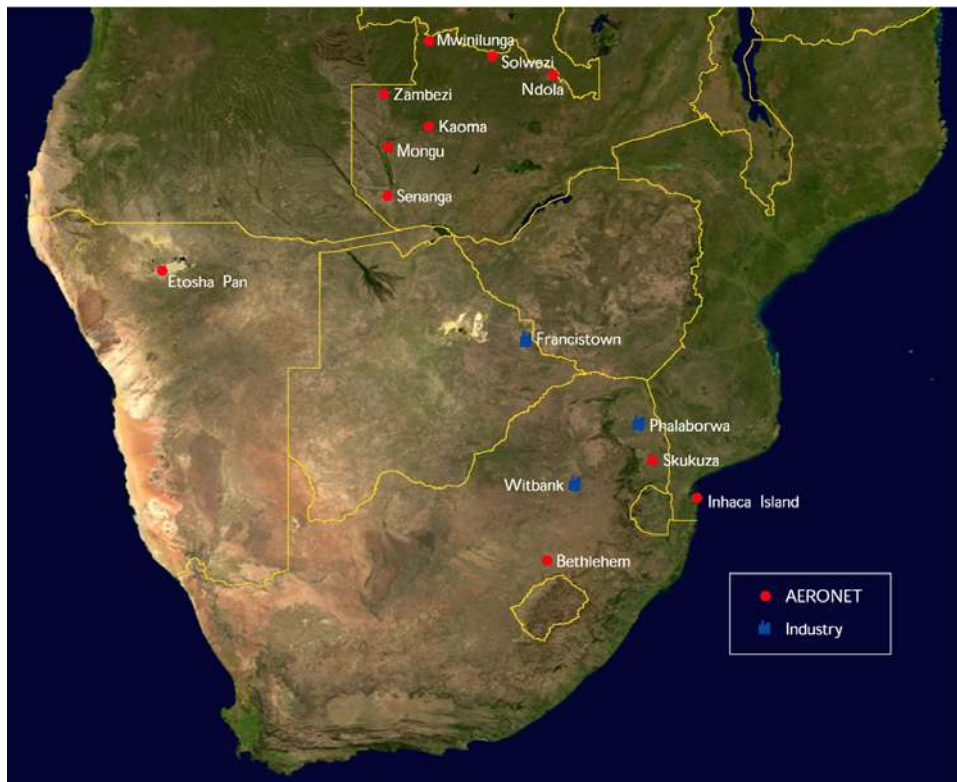
Figure 1. MODIS satellite image map of southern Africa showing the location of AERONET Sun/sky radiometer sites in August–September 2000 that were analyzed in this study, and with regional industrial centers also identified.

change in calibration with time was assumed in the interpolation between the two calibrations. The combined effects of uncertainties in calibration, atmospheric pressure (not monitored), and total ozone amount (climatology is used) result in a total uncertainty of ~0.010–0.021 in computed τ_a for field instruments (which is spectrally dependent with the higher errors in the UV [*Eck et al.*, 1999]). The effect of forward scattered diffuse radiation within the 1.2° field of view of the Sun photometer has also been considered. Simulations by *Kinne et al.* [1997] show that for aerosol particles with effective radius of 0.2 μm (similar in size to biomass burning aerosols), there is essentially no measured effect on aerosol optical depth, even for Sun photometers with a 2° field of view. *Schmid et al.* [1999] compared τ_a values derived from 4 different solar radiometers (one was an AERONET Sun-sky radiometer) operating simultaneously together in a field experiment and found that the τ_a values from 380 to 1020 nm agreed to within 0.015 (rms), which is similar to our estimated level of uncertainty in τ_a retrieval for field instruments.

[8] In Mongu, Zambia measurements of broadband Photosynthetically Active Radiation (PAR; 400–700 nm) downwelling fluxes were made with a Skye-Probetech SKE-510 instrument. These measurements of PAR flux were made at a 2 minute sampling interval and the data were transmitted to the METEOSAT satellite along with the CIMEL Sun-sky radiometer data. Another transient SKE-510 PAR flux sensor was operated side-by-side in Mongu for 2 weeks during the experiment, and the calibration of that instrument was transferred to the monitoring instrument in Mongu by comparison

of data taken coincidentally in space and time. The calibration of the transient PAR sensor was checked by comparison with cloudless sky flux computations (6S model [*Vermote et al.*, 1997]) under cloudless conditions in Mongu on 29 August 2000 when the τ_{a500} = 0.13 and also at GSFC, Maryland after immediately returning from SAFARI 2000 on 29 September 2000 when τ_{a500} = 0.08. The agreement between the flux model computations and the PAR measurements in both of these sites/cases was within 1% or less. *Eck et al.* [2001] have discussed that any assumptions made about the aerosol optical or surface reflectance characteristics under such a low aerosol loadings resulted in an uncertainty in 6S computed PAR fluxes of <1%.

[9] Also in Mongu, spectral total and diffuse irradiance was measured in six narrow spectral bands, 10 nm full-width half-maximum bandpass, with a Yankee Environmental Systems, Multi-Filter Rotating Shadowband Radiometer (MFRSR). The MFRSR took measurements at 415, 496, 615, 672, 870 and 939 nm, sampled at 1 to 4 minute intervals (varying on different dates), with no averaging of the measured values. Instrument calibration of the MFRSR was not an issue in our study, since analysis was performed on only the diffuse faction (diffuse/total irradiance) measurements, with the same detector (silicon photodiode) measuring both of these components of the spectral irradiance.

2.3. Analysis Methodology

[10] The CIMEL sky radiance almucantar measurements at 440, 675, 870, and 1020 nm in conjunction with the direct Sun measured τ_a at these same wavelengths were
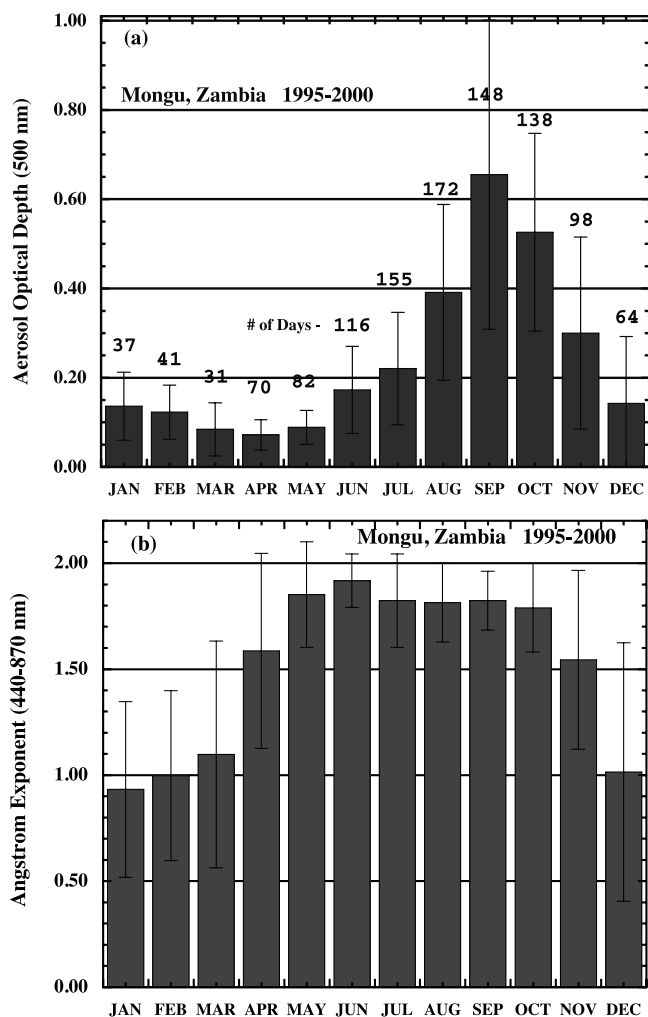
Figure 2. (a) The multiannual monthly means of τ_{a500} from 1995 to 2000 for Mongu, Zambia. The number of days of observations for each month are given, with many more observations made during the dry season biomass burning months due mainly to lack of monitoring in the wet season, but also due to extensive cloudiness in December–April. (b) Multiannual monthly average Angstrom wavelength exponents at Mongu (computed from linear regression of ln τ_a versus ln λ with 440, 500, 675, and 870 nm data) for the same data as shown in (a).

used to retrieve aerosol size distributions following the methodology of *Dubovik and King* [2000]. Almucantar sky radiance measurements were made at optical air masses of 4, 3, and 2 in the morning and afternoon, and once per hour in between. Spherical particle shape is assumed in the retrievals; a reasonable assumption for smoke aerosol as the measurements of *Martins et al.* [1998] showed that particles in Amazonian regional smoke hazes were largely spherical. The same instrumentation as was used by *Martins et al.* [1998] in Amazonia was also utilized in southern Africa during SAFARI 2000 on the CV-580 aircraft and the data did not show any appreciable particle asphericity (P. V. Hobbs, private communication, 2002). In order to eliminate cloud contamination from the almucantar data we require the radiances to be symmetrical on both sides of the Sun at

equal scattering angles. We eliminate scattering angle radiance pairs that are not symmetrical and require that a minimum of 21 angles remain out of a maximum total of 27 angles. Sensitivity studies performed by *Dubovik et al.* [2000] were used to analyze the perturbations of the inversion resulting from random errors, possible instrument offsets and known uncertainties in the atmospheric radiation model. Retrieval tests using known size distributions demonstrated successful retrievals of mode radii and the relative magnitude of modes for various types of size distributions such as bimodal accumulation mode dominated aerosols and bimodal coarse mode dominated aerosols. Simultaneous retrievals of aerosol single scattering albedo are also made with this algorithm and the sensitivity analysis shows that these retrievals have an uncertainty of ∼0.03 for biomass burning aerosols when is $\tau_{a440} \geq 0.5$ [*Dubovik et al.*, 2000]. Both the single scattering albedo and size distributions retrieved from this algorithm are representative of the aerosol optical properties integrated over the entire atmospheric column. Therefore they should be considered as the radiatively effective column-integrated values of these parameters.

3. Spectral Aerosol Optical Depths
3.1. Seasonal, Temporal, and Spatial Variability Within Zambia

[11] In order to characterize the seasonal duration of biomass burning in western Zambia, we have analyzed the data from our long-term AERONET monitoring site in Mongu. This data set spans the burning seasons of 6 years (1995–2000) and the wet seasons for 2 years (1999–2000). All τ_a data presented in this paper have been screened for clouds following the methodology of *Smirnov et al.* [2000] which relies on the greater temporal variation of cloud optical depth versus aerosol optical depth. These monthly mean τ_{a500} values presented in Figure 2a represent an additional 2 year update to the multiyear climatological τ_a statistics presented by *Holben et al.* [2001]. It is noted that the dry season months of April–October in Mongu contribute < 10% of the long-term mean annual rainfall. The smoke τ_{a500} increases gradually at first from the preburning season monthly mean in April of 0.07 to an annual peak in September of 0.65, then decreases steadily to a nearly background level again in December. The corresponding monthly mean Angstrom exponents are shown in Figure 2b. These α values were computed from linear regression of ln τ_a versus ln λ for measurements taken at 440, 500, 675, and 870 nm. The high values of average α from April through November (>1.5 for all months) indicate that the aerosol is dominated by accumulation mode radius (r < 0.6 μm) particles. These fine mode particles may be produced by biomass fuel cooking fires in April–May but as the dry season progresses, increasingly more landscape level biomass burning associated with agricultural practices dominates. The relatively low α values of December–March (monthly means = 0.9 to 1.1) indicate a significant contribution of coarse mode particles. Since rainfall in Zambia is quite heavy during this period, resulting in high soil moisture and filling seasonal lakes and pans, it is unlikely that locally generated aeolian dust is a significant contribution to the coarse mode. The coarse mode aerosols during
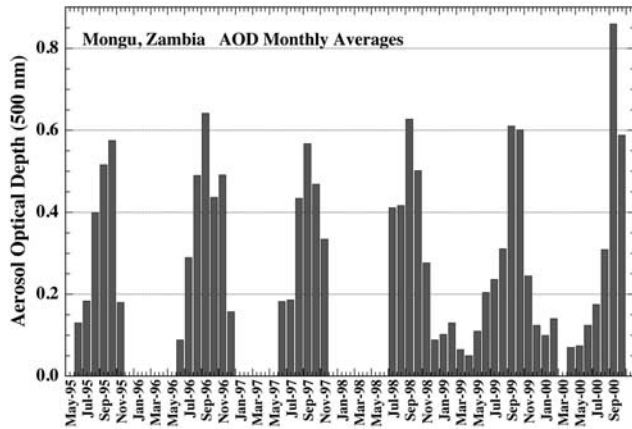
Figure 3. Individual monthly means of τ_a at Mongu, Zambia shown for May 1995 through October 2000, which indicate large interannual variability in some months (i.e., September in 2000 versus all other years).

the wet season may be partly composed of biogenically produced particles. However, a small amount of cloud contamination during these cloudy rainy months may also contribute to lower α values since $\alpha \approx 0$ for clouds, and since τ_a is quite low.

[12] The monthly means of τ_{a500} for each month from 1995 to 2000 are shown in Figure 3 to more clearly illustrate the inter-annual variability in τ_a. Significant inter-annual variability occurs at Mongu, as was noted by *Holben et al.* [2001], resulting from variability of the large scale circulation and in the timing and extent of rainfall (for the end of the burning season in November). The months of August and September 2000 (SAFARI 2000) exhibit monthly average τ_a values which deviate significantly from the means of the previous five years. The August 2000 monthly average τ_a is lower than the mean of the previous 5 years but similar to the August 1999 value. However, the September 2000 mean is significantly higher than that of any month for the previous 5 years. The large increase in the monthly average τ_a from August to September is due to a shift in atmospheric circulation patterns. These months generally represent a transition from the dry season, characterized by the northern boundary of the central Botswana anticyclone, and the wet season, dominated by moist air advected from the northwest along the Congo air boundary. Meteorological conditions during the SAFARI 2000 dry season campaign (August–September 2000) are discussed in detail by D. C. Stein et al. (Haze layer characterization and associated meteorological controls along the western coastal region of southern Africa, submitted to *Journal of Geophysical Research*, 2002) (hereinafter referred to as Stein et al., submitted manuscript, 2002).

[13] The difference between monthly average τ_{a500} from August to September 2000 for Mongu is also seen to occur for 5 other sites in western Zambia (Figure 4). For the month of August (days 214–244) the daily average τ_a shows relatively little variability and much lower magnitude values than occurred in September. A north-south gradient in τ_a was observed in August, with highest values in the north. A similar gradient was also observed in Zambia during part of August–September in 1997 [*Eck et al.*,

2001]. *Scholes et al.* [1996] estimated that the amount of biomass burned in southern Africa had a strong north-south gradient resulting partly from a strong north-south gradient in rainfall and thus resulting in greater vegetation production in the north. Satellite detected fire counts also show a north-south gradient in this region, with few fires detected south of Zambia's southern border [*Justice et al.*, 1996]. However, in September this north-south gradient in τ_a was not maintained during two major smoke transport events which dominated the month [*Annegarn et al.*, 2002], although the north-south gradient appeared to be reestablishing at the end of September when monitoring ceased for all Zambian sites except Mongu.

[14] The spectral variation of τ_a at Mongu during a large part of the SAFARI 2000 campaign (23 August to 16 September 2000) is shown in Figure 5. The Angstrom exponent values generally decrease as τ_a increases although not in exact correlation. The α computed from the shorter wavelength pair of 380–500 nm (Figure 5b) exhibited much greater dynamic range than the longer wavelength pair α values computed from 500 to 870 nm data (Figure 5b). This is a result of the short wavelength α being much more sensitive to fine mode particle size [*Reid et al.*, 1999] and the correlation of fine mode radius with τ_a at this site [*Eck et al.*, 2001]. The AERONET volume size distribution retrievals [*Dubovik and King*, 2000] of August–September 2000 at Mongu and Senanga show that the peak fine mode radius increases as τ_a increases (while the coarse mode exhibits relatively little systematic change in amplitude or size), similar to that observed in Mongu during the 1997 ZIBBEE campaign [*Eck et al.*, 2001]. The rate of change of α with wavelength ($d\alpha/d \ln \lambda$) or α' also shows a strong relationship with τ_a magnitude (Figure 5c) since α' increases as the fine mode increasingly dominates over the coarse mode [*Eck et al.*, 1999] and as the fine mode radius increases [*Eck et al.*, 2001]. The fine mode radius typically increases as τ_a increases due to aging processes (coagulation, condensation, and gas-to-particle conversion) resulting in fine mode particle growth as τ_a builds in concentration [*Reid et al.*,
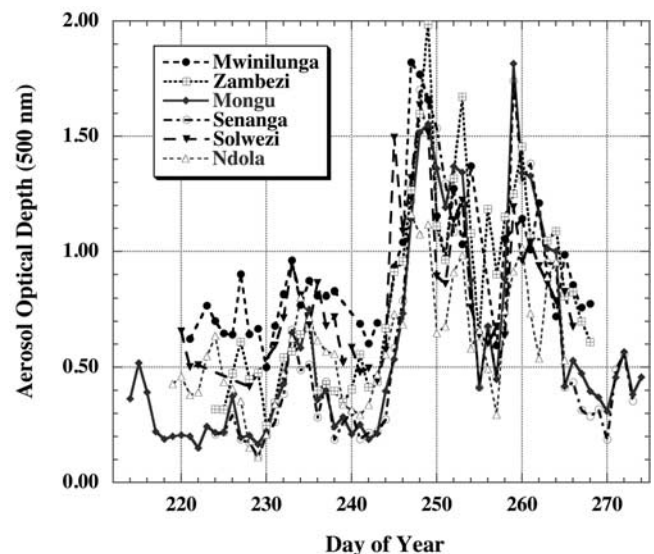

Figure 4. Daily average values of τ_{a500} for six sites in Zambia during August–September 2000.
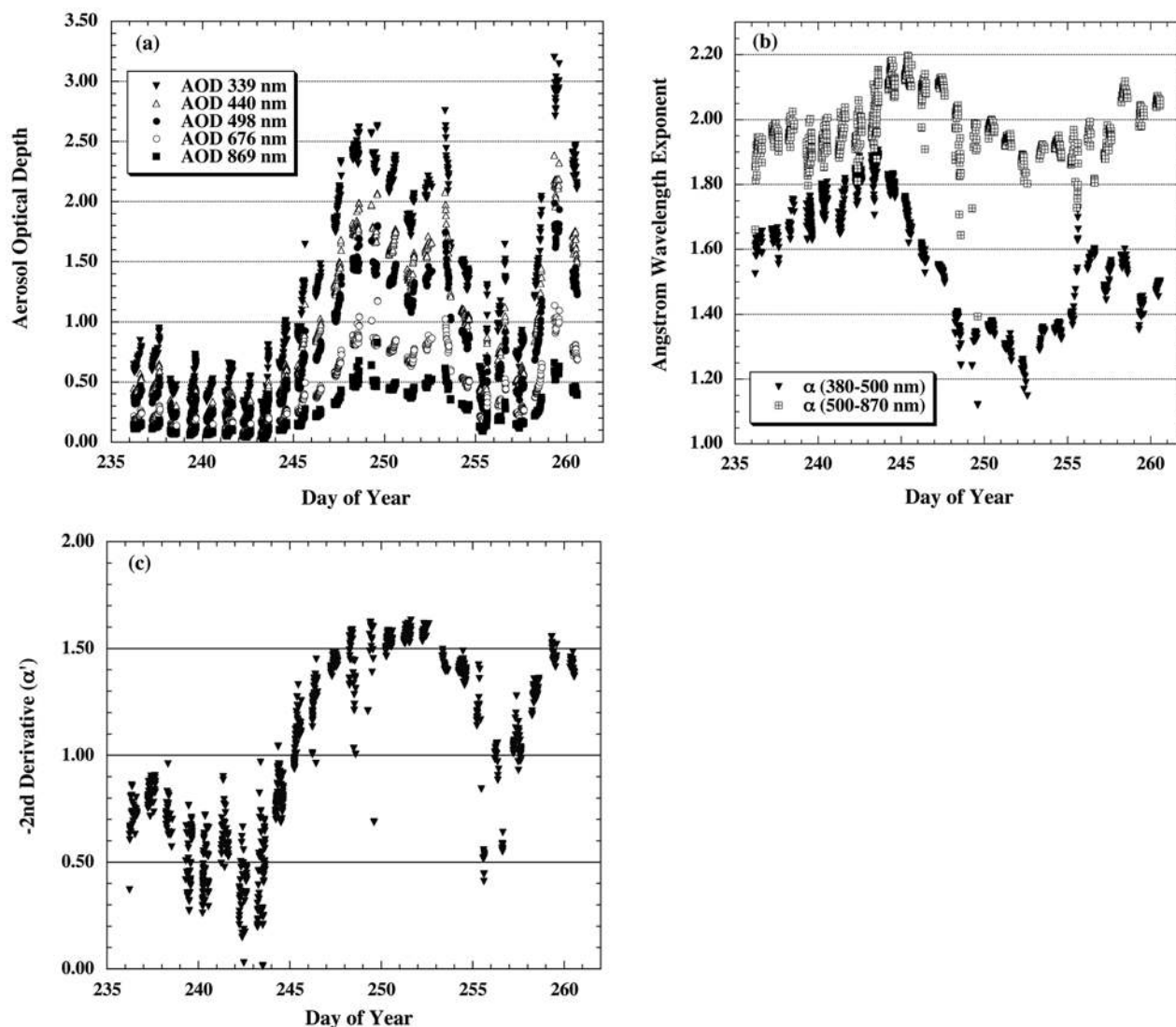
Figure 5. (a) The spectral variation of instantaneous measurements of τ_a at Mongu for 23 August to 16 September 2000 showing the gradual buildup and decline of smoke concentrations in this period. (b) The short wavelength pair Angstrom exponent $\alpha_{380-500}$ and the longer wavelength pair $\alpha_{500-870}$ for the same data as was shown in (a). (c) Instantaneous values of α' ($d\alpha/d \ln\lambda$) for the same data as in (a), showing dynamic variations as a result of both increasing (decreasing) fine mode particle size and greater domination of fine mode versus coarse mode optical depth as τ_a increases (decreases).

1998]. Aerosol hygroscopic growth may have contributed to the increase in fine mode particle size as τ_a increased but this influence is likely to have been small since the aerosol layer relative humidity over land was generally low in this season [*Haywood et al.*, 2003] in relation to the relative humidity required for significant hygroscopic growth [*Magi and Hobbs*, 2003].

[15] The time series of both τ_{a500} and total column precipitable water vapor (PWV) for August–September 2000 in Mongu are shown in Figure 6. Although there is some correlation between the instantaneous magnitudes of PWV and τ_a for this time period, they are also significantly out of phase during the two major events of aerosol increases associated with transport in September. Compared to a 3 week period in August–September 1997 where PWV and τ_a at Mongu were highly correlated ($r^2 = 0.76$ [*Eck et*

al., 2001]) the correlation for August–September 2000 is quite low ($r^2 = 0.27$). It is noted that there was similar low correlation between PWV and τ_a at all 5 other Zambian sites for the same time period in 2000. The simple explanation of northerly flow advecting air that has both higher aerosol loading and higher PWV does not seem to hold. Figure 7 shows TOMS instrument Aerosol Index (AI) for southern Africa with 700 mb streamlines from the USA National Meteorological Center (NMC) reanalysis superimposed for 1–8 September 2000. The streamlines are representative of the wind field at ~2 km above the surface at Mongu (black triangle on maps) since the streamline geopotential heights are ~3100 m. *Hsu et al.* [1999] has shown that the AI is highly correlated with τ_{a380} from AERONET data at Mongu during the July–October 1996 and 1997 burning seasons. From examination of these 700 mb wind fields it is seen that
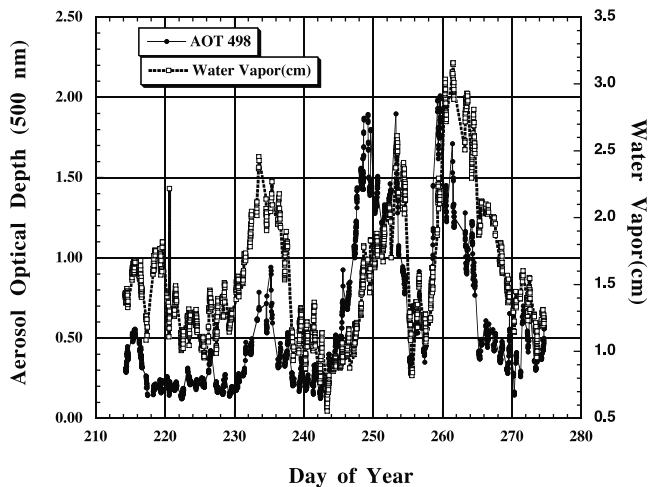
Figure 6. The time series of both τ_{a500} and total column precipitable water vapor (PWV) at Mongu for August–September 2000. Note that the τ_{a500} and PWV are out of phase in September (Days 245–274).

the increase in aerosol loading starting on 1 September is associated with a northerly flow component. Prior to 1 September similar maps show the areas of highest AI values located persistently to the north and west of Mongu. At the maximum aerosol loading day for this event, 5 September, Mongu is under the northern ridging effect associated with the Botswana anticyclone. The subsidence and divergence associated with this high pressure system may result in lower PWV concentrations at this time of maximum aerosol loading, and the strong subsidence may also inhibit the vertical transport of aerosols. However, it is difficult to explain all of the variation in τ_a and PWV based on the NMC streamline analyses alone, perhaps in part due to some uncertainty in the analysis due to the very sparse network of radiosonde stations, particularly in the northern half of the region.

3.2. Optical Depth Variability in the Southern Africa Region During SAFARI 2000

[16] The time series of τ_{a500} for August–September 2000 for five continuously monitoring AERONET sites from ∼15° S (Mongu) to ∼28° S (Bethlehem) are shown in Figure 8. Through most of the month of August (Day 214–244) there is not a very large gradient in τ_{a500} throughout this extensive region. On many days in August the total range in τ_{a500} for all 5 sites is only ∼0.25 or less. In addition there is some coherence in the local maxima and minima of τ_{a500} for all sites, suggesting the influence of a regional scale circulation pattern affecting the entire area. This spatial coherence changes markedly in September when air with very high aerosol concentration moves southward to varying degrees (Figure 7). The gradient in τ_{a500} exceeds 1.50 on some days, with highest values in Mongu (northernmost), and lowest in Bethlehem (southernmost). The high optical depth smoke plume is advected to the southeast over southern Africa, exiting the continent right over Inhaca Island from 2 to 6 September 2000, but not reaching as far south as Bethlehem (Figure 7). However, from 13 to 16 September, the circulation pattern is shifted

farther to the south and on a couple of these days the τ_{a500} at Bethlehem exceeds the values measured at Skukuza and Inhaca since the smoke plume is exiting the continent into the Indian Ocean to the south of Inhaca. The τ_{a500} time series at Etosha Pan shows a pattern that is quite different from Mongu even though it is the closest in latitude to Mongu of the 4 sites. On a few days the τ_{a500} at Etosha even exceeds the values at Mongu. TOMS maps of AI show that this occurs when smoke is advected in an anticyclonic pattern from the region north of Mongu, over Angola (the country with maximum burning during SAFARI 2000), out to the Atlantic and then back inland to the east and south of Mongu.

[17] During the two large transport events in September it is noted that the smoke optical depths at Inhaca and Skukuza are typically 50% or less than the values measured at Mongu (Figure 8a), due to large scale dispersion, diffusion and also dry deposition which occur during long range transport. Although the TOMS Aerosol Index has higher values over Skukuza and Inhaca than over Mongu on 4–5 September, these high values of AI are the result of smoke overriding brightly reflecting cloud tops, thereby enhancing the UV multiple reflections within the smoke and molecular atmosphere [*Torres et al.*, 1998]. Lidar data from the Skukuza site on these dates shows the presence of aerosol at altitudes above low level broken clouds (E. J. Welton, private communication, 2002).

[18] The time series of the daily average Angstrom exponents (computed from linear regression of ln τ_a versus ln λ for 440, 500, 675, and 870 nm) for the same sites and dates as Figure 8a is shown in Figure 8b. We have selected a wide range of wavelengths (visible to near infrared) to compute the Angstrom exponent for this particular regional comparison in order to have more sensitivity to the relative amount of coarse mode aerosol contribution to the total aerosol optical depth [see *Reid et al.*, 1999; *Eck et al.*, 1999; *O'Neill et al.*, 2001]. The northernmost site, Mongu, has the highest α values on the majority of days, typically ranging from ∼1.7 to ∼2.1. This results from Mongu being located in the most active biomass burning region of all sites and closest to the region of maximum biomass burning emissions north of Zambia. Therefore the aerosol in Mongu is dominated by fine mode smoke and also is the least aged smoke of all of these sites. The lower α values at the other sites suggest a more aged smoke aerosol (growth of fine mode particles) and/or a greater coarse mode contribution from other types of aerosols. The lowest α of all of these sites occurred at Inhaca Island which is only ∼200 km southeast of Skukuza. Inhaca Island is located in the Indian Ocean ∼40 km directly east of Maputo (population ∼1 million), the capital of Mozambique. Therefore the Inhaca Island site is exposed to marine aerosol, such as coarse mode dominated sea salt, that is largely lacking from the other site locations in South Africa in this season [*Piketh et al.*, 1999]. The larger relative humidities of the maritime air may also result in hygroscopic aerosol growth at Inhaca that would not occur at the very low humidity inland sites during these dry season months. Additionally, since this is the only site in our study in relatively close proximity to an urban center, the emissions from the activities in this region (industrial activity) may contribute to the larger sized particles (lower α) at Inhaca. A more in-depth discussion of the aerosol

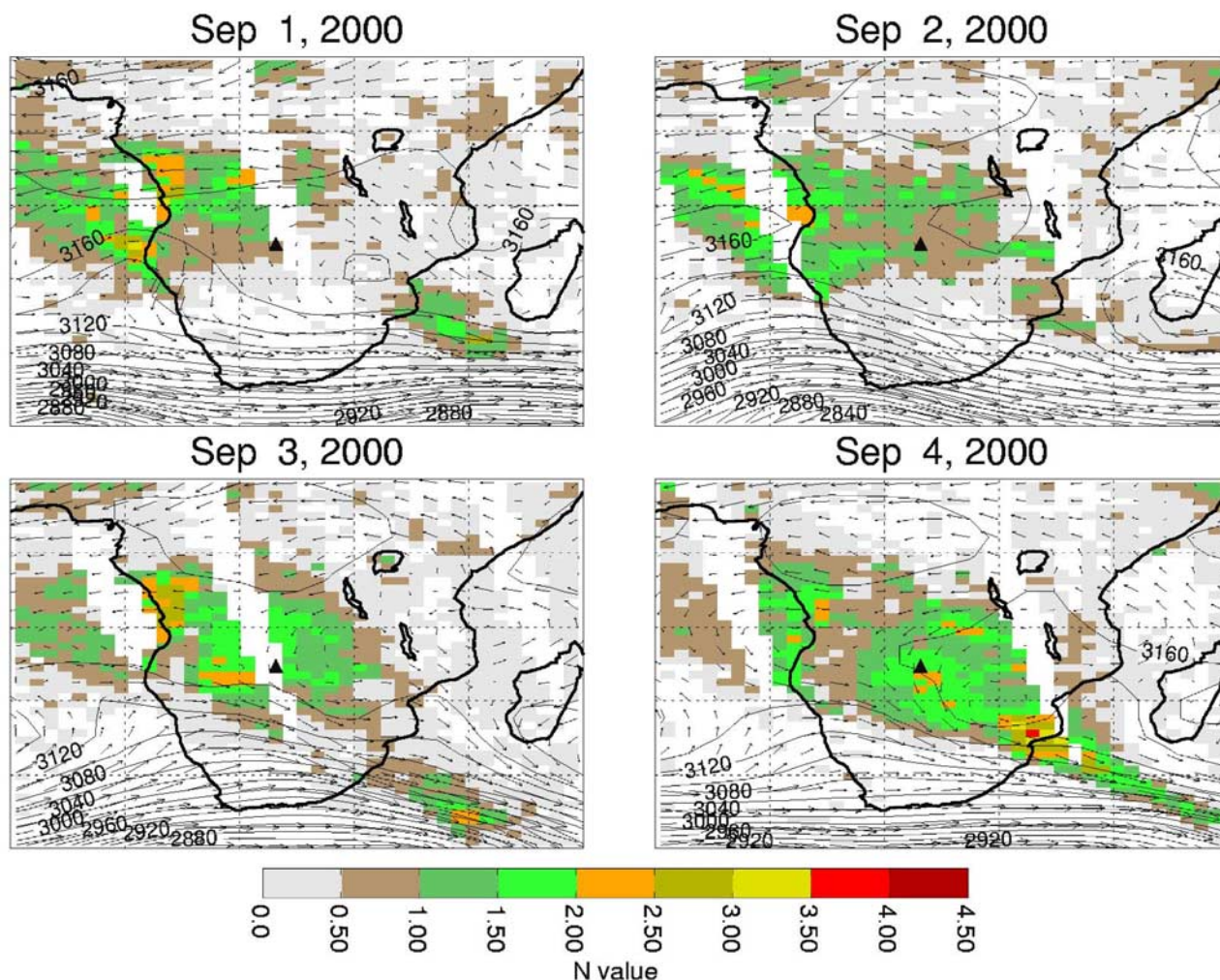# TOMS Aerosol Index and NMC REAN 700mb streamline

Figure 7. TOMS-derived aerosol index and National Meteorological Center 700 mbar streamline analysis for 1–8 September 2000. Geopotential height values in meters and the wind vectors at this level are also shown. The black triangle at the center of each panel is the location of Mongu, Zambia.

optical properties at Inhaca is given by *Queface et al.* [this issue]. We will further analyze the comparison of aerosol particle sizes between sites when we examine the almucantar retrieved size distributions in section (4).

[19] The mean diurnal variability of τ_{a500} expressed as percent difference from the daily mean, versus the time of day is shown in Figure 9. Data were analyzed for the six sites in Zambia and the other four long-term monitoring sites in southern Africa. At each site the mean τ_{a500} for each day was computed and then the percent difference from that for each observation was calculated, and averaged in hourly bins. The percent departures from daily mean for each hour were then averaged over the whole two month period, August–September 2000. All six of the sites in Zambia showed a significant average diurnal trend with minimum τ_{a500} at 0900 UTC (1100 local time) and maximum at 1500 UTC (1700 local time). Actual maximum τ_{a500} may occur later but no later observations are possible due to sunset. This diurnal cycle in aerosol loading is possibly caused by a diurnal cycle in the number of biomass burning fires and

their intensity. There was no significant diurnal variability of Angstrom exponent (440–870 nm), so this afternoon increase in AOD is not due to an aeolian dust contribution. Higher air temperatures, lower relative humidity, and higher wind speeds at midday and afternoon may result in more intense and faster moving fires at those times of day. Agriculturalists take advantage of these favorable conditions and start more fires beginning in the late morning. *Prins et al.* [1998] have utilized the 3.7 μm channel on the GOES geostationary satellites to monitor the diurnal cycle of burning in the tropical rain forest and cerrado (savanna) regions of South America. They found a strong diurnal cycle in fire counts with an approximate doubling from 1445 to 1745 UTC (late morning to early afternoon). For southern Africa, the 3.7 μm radiance data from the Tropical Rainfall Monitoring Mission (TRMM) satellite also indicate a strong diurnal cycle in fire counts in August–September with the maximum number of fires occurring ~3 hours after local solar noon (~1300 UTC; L. Giglio, personal communication, 2002).

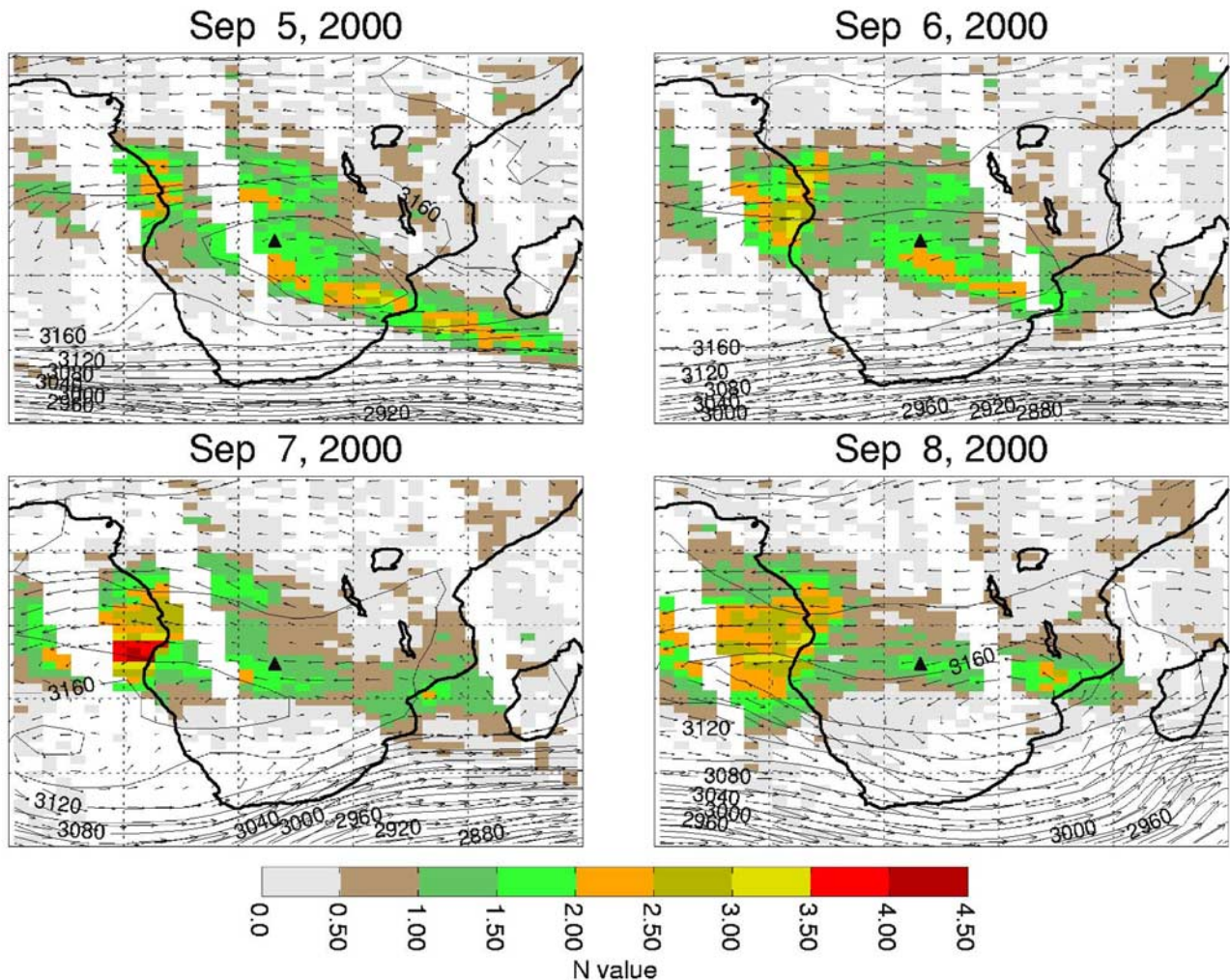## TOMS Aerosol Index and NMC REAN 700mb streamline

Figure 7.   (continued)

[20]   In contrast to the Zambian sites, all of the other sites (Etosha Pan, Skukuza, Inhaca, and Bethlehem) show relatively small mean diurnal variability (Figure 9). The variability for all of these sites is within ±5% of the daily mean, except for 1 hour at Skukuza (1400 UTC) which is at +12%. Since these sites are not in as active biomass burning regions as Zambia, it is likely that more of the diurnal variation in τ_{a500} would be due to aerosol advection by winds from distant source regions. Advection and the related synoptic scale meteorological patterns are not likely to have a repeatable diurnal cycle, thereby resulting in relatively random diurnal variability of τ_{a500}. This is not to say that the diurnal variation of τ_{a500} is not significant on some days, but only that there is no mean diurnal pattern in τ_{a500}. The increase in τ_{a500} for the last 2 hours of the day at Skukuza may be related to local savanna burning in the region around the site since fire is used for agricultural land clearing and for ecological management of the national park (Kruger) and game reserves in this region. *Kaufman et al.* [2000] discusses various aspects of the differences between daily average τ_a and values measured at the

satellite overpass times of Terra and Aqua (late morning and early afternoon, respectively). Although this ensemble analysis of data from ∼70 globally distributed AERONET sites over 7 years suggests that there is relatively little systematic diurnal variation, on a regional scale the average diurnal cycle of τ_a can be significant.

4.   Column-Integrated Aerosol Size Distribution Comparisons

[21]   In this section we present and analyze volume size distribution retrievals obtained from the application of the *Dubovik and King* [2000] algorithm to spectral almucantar sky radiances and spectral τ_a from the CIMEL Sun-sky radiometers. Comparisons of the radiatively effective column-integrated aerosol volume size distribution retrievals from six sites in Zambia are made, in addition to comparison of these size distributions to those of other sites in the region (Inhaca, Skukuza, Etosha, and Bethlehem).

[22]   First, however, we compare these AERONET measured retrievals to those made by in situ sampling with
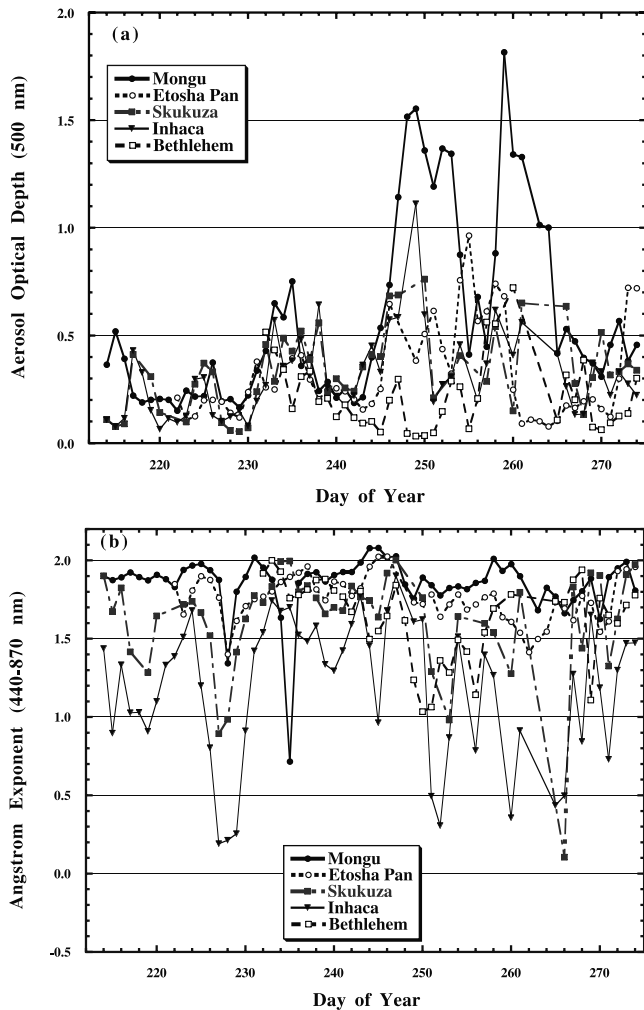
Figure 8. (a) The time series of daily average τ_{a500} for August–September 2000, for five widely distributed sites in the southern Africa region (see map of Figure 1). (b) Time series of daily average α (computed from linear regression of ln τ_a versus ln λ for 440, 500, 675, and 970 nm data) for the same data as shown in (a).

aircraft instrumentation for cases of biomass burning aerosols. During the Smoke Clouds and Radiation-Brazil (SCAR-B) experiment in August–September 1995, the University of Washington C-130 aircraft made numerous sampling flights of the biomass burning smoke aerosol. The Differential Mobility Particle Sizing (DMPS) instrument data from these flights were utilized by *Reid et al.* [1998] to characterize the lognormal volume size distributions of the accumulation mode particles. In Figure 10 we compare the lognormal size distribution of *Reid et al.* [1998] for local smoke in Cuiaba, Brazil to the lognormal cerrado smoke model of *Dubovik et al.* [2002]. The region surrounding Cuiaba is composed of agricultural lands and cerrado, which is a South American vegetation classification that is very similar to savanna. Most of the data that was utilized to compute the Dubovik cerrado model was from the AERONET site in Cuiaba for the years 1993–1995. The Dubovik et al. size distribution model is dynamic in τ_a (particle size increases as τ_a increases), and a value of $\tau_{a440} = 1.0$ was

chosen to be representative of aerosol loading from local burning. This is similar to the level of aerosol loading which occurred during the SCAR-B flights analyzed by *Reid et al.* [1998]. This comparison of lognormal size distributions (Figure 10) shows excellent agreement in particle modal radius and standard deviation of the accumulation mode. The modal radius differ by only ~0.01 μm and the geometric standard deviation are nearly equal at 1.58 (Reid) and 1.60 (Dubovik).

[23] An additional comparison of in situ measured size distribution from an aircraft platform and the AERONET retrievals was made by *Haywood et al.* [2003]. Their C-130 aircraft flew an altitudinal profile over the AERONET site at Etosha Pan on 13 September 2000 as a part of the SAFARI 2000 campaign. This single day comparison shows excellent agreement in accumulation mode radius and geometric standard deviation, considering the temporal variability and uncertainties in both the retrieved size distribution from AERONET measurements [*Dubovik et al.*, 2000] and for the in situ measurements made with the PCASP instrument on the C-130 aircraft [*Haywood et al.*, 2003]. Thus for the case where one type of atmospheric aerosol particles (biomass burning) dominate and the aerosol layer is well mixed, there is very good agreement between the in situ measurement of aerosol size distribution and the remote sensing retrievals made by AERONET.

[24] During the SAFARI 2000 dry season campaign (August–September 2000), there was a similar trend of increasing particle radius as τ_a increased as was observed during the Zambian International Biomass Burning Emissions Experiment (ZIBBEE) in Mongu in August–September 1997 [*Eck et al.*, 2001]. The peak in the accumulation mode volume radius increased from ~0.12 μm at $\tau_{a440} \approx 0.2$ to ~0.16 μm for $\tau_{a440} \approx 1.6$. This radius increase with increasing τ_a may be due to particle growth associated with aging from a combination of coagulation, condensation, and
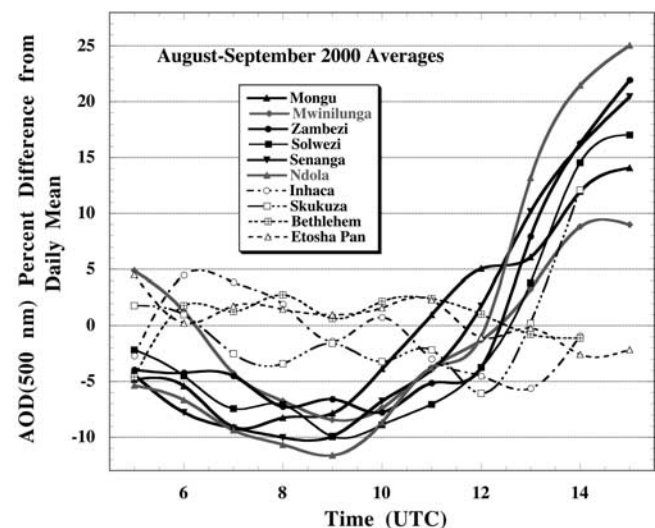

Figure 9. Mean diurnal variability of τ_{a500} expressed as the percent difference from the daily mean versus hour of the day for August–September 2000. All six sites in Zambia (solid lines) show significant diurnal variability while the other sites to the south exhibit little variability.
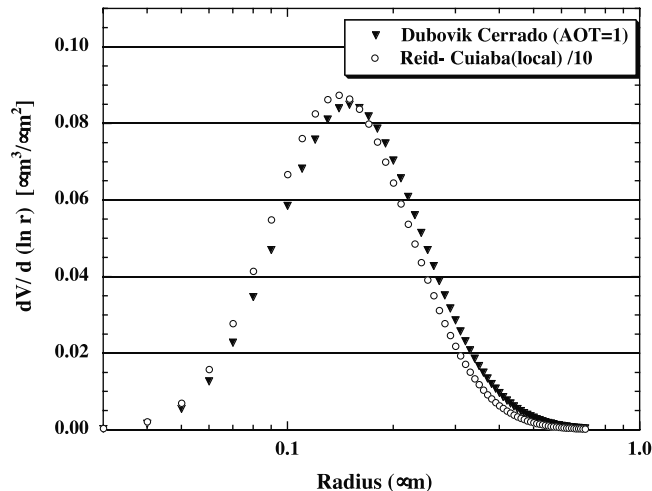
Figure 10. Comparison of the normalized fine mode biomass burning aerosol lognormal size distribution from in situ measurements of local smoke in Cuiaba, Brazil [*Reid et al.*, 1998] to the lognormal cerrado (Brazil) smoke model of *Dubovik et al.* [2002], for τ_{a440} = 1.0.

gas-to-particle conversion [*Reid et al.*, 1998]. Hygroscopic particle growth may also contribute to the observed increase in radius, however relative humidities are generally quite low during these dry season months thereby limiting this growth mechanism.

[25] A comparison of size distribution retrievals made on one day (3 September 2000), for 6 sites in Zambia is shown (Figure 11) to examine the spatial variability of particle size on the regional scale ($\sim$450 km north-south and $\sim$600 km east-west). Data from Mwinilunga is not shown since it was cloudy at that site on 3 September. The aerosol loading is relatively similar over the six sites on this day with τ_{a440} ranging from 1.25 to 1.54, thus reducing the influence particle size change as a function of τ_a. The accumulation mode (radius <0.5 μm) size distributions are quite consistent for all sites with little difference in the value of peak modal radius (range 0.145 to 0.155 μm) and the geometric standard deviation ranging from 1.51 to 1.61 with an average of 1.55. There is more variation in the coarse mode size distributions, with the easternmost sites (Ndola and Solwezi) exhibiting greater coarse mode magnitude. However, the coarse mode contribution to the aerosol optical depth at 440 nm ranges from only $\sim$0.02–0.04 for all six sites. Differences in the magnitude of spectral single scattering albedo and small differences in the particle size distributions account for the range of extinction aerosol optical depths at these sites on this day. Similarly a comparison of average size distributions at six sites in Zambia for August–September 2000 for τ_{a440} ranging from $\sim$1.0 to 1.1 ($\sim$10 to 12 almucantar retrievals averaged per site, measured on different days) showed very little variation in accumulation mode size between sites and also very consistent coarse mode distributions. Therefore on a limited regional scale, within west-central Zambia, there appears to be little variability in the size distribution of the biomass burning aerosols for a given level of aerosol loading or τ_a.

[26] A comparison of aerosol size distributions on a more extensive regional scale, encompassing the sites in Nami-

bia, South Africa, Mozambique, and Zambia is shown in Figure 12. A comparison of these sites at an aerosol loading resulting in τ_{a440} of 0.75 to 0.77 for August–September 2000 is shown in Figure 12. The size distributions shown here are computed from an average of 10–13 individual almucantar scan retrievals made over several days. This level of aerosol loading is representative of the upper range of τ_a observed at Skukuza and Inhaca, and close to the monthly mean for September for Senanga. The accumulation mode sized particles are similar for all four sites for this data sample, with a variation of only $\sim$0.01 μm in volume radius, even though there may be significant contributions from fossil fuel burning and industrial emissions at Skukuza and Inhaca. The coarse mode on the other hand exhibits significant differences in size and width of the mode, and also large differences in the relative magnitude of the fine to coarse mode between sites. The coarse mode particles at both Inhaca and Skukuza are shifted toward smaller size and a broader width than observed at Senanga and Etosha. This is consistent with the lower Angstrom exponent observed at these two sites (especially Inhaca; see Figure 8b) possibly resulting from additional contribution of aeolian dust and fly ash to the aerosol mixture and also of sea salt at Inhaca Island. The size distributions at Senanga and Etosha are very similar, both dominated by fine mode biomass burning aerosols with a slightly enhanced coarse mode at Etosha.

[27] At a lower aerosol loading of τ_{a440} = 0.42–0.44 similar differences are observed in the coarse mode as were noted at the higher aerosol loading. Again both Skukuza and Inhaca exhibit a shift toward smaller sized coarse mode particles and a much broader width than for Senanga and Etosha. At $\tau_{a440} \approx 0.43$ the fine mode particle size at Inhaca and Senanga are significantly smaller, possibly due to a greater contribution of fresh smoke (less aged) at Senanga and possibly a greater contribution of pollution from nearby Maputo city at Inhaca. However, multiyear statistics should be analyzed to explore these possibilities since for a sample from only a few days at each site the air mass history and
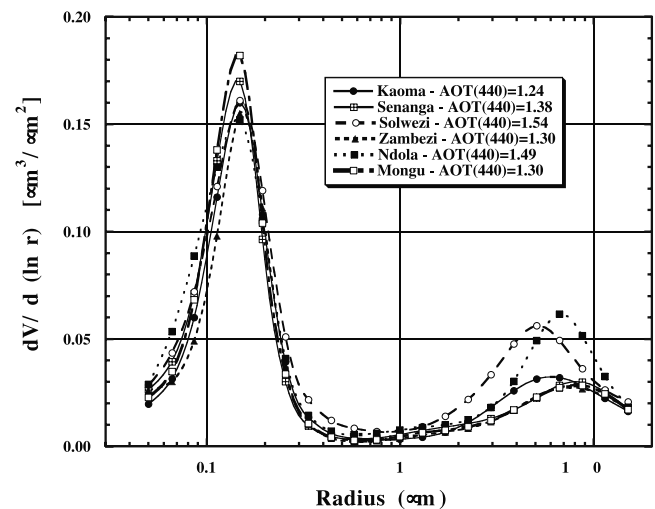

Figure 11. AERONET volume size distribution retrievals made on 3 September 2000 for six sites in Zambia (distributed $\sim$450 km north-south and $\sim$600 km east-west).
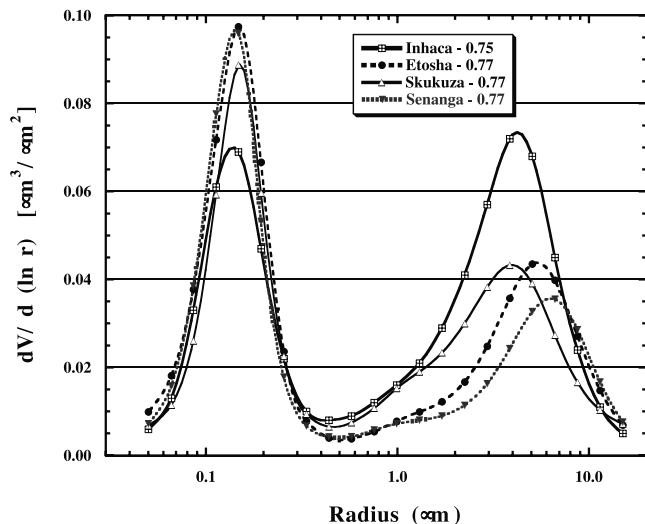
Figure 12. Regional comparison of mean aerosol volume size distributions for sites in South Africa, Mozambique, Namibia, and Zambia for August–September 2000 when average τ_{a440} = 0.75–0.77. Each size distribution is computed as an average from 10 to 13 individual almucantars per site.

local meteorology may exhibit a significant influence that may not be considered typical or representative.

5. Column-Integrated Aerosol Single Scattering Albedo Comparisons

[28] Retrievals of the spectral single scattering albedo at 440, 675, 870, and 1020 nm were made by application of the *Dubovik and King* [2000] algorithm to almucantar sky radiances and direct Sun τ_a retrievals in these wavelengths. In this section we will present analysis of the variability of these retrieved ω_0 values during SAFARI 2000 for the same sites which we discussed regarding size distributions in the previous section. We also present analysis of the single scattering albedo retrieved from two other ground based remote sensing methods and compare these to the AERONET retrievals. One of these methods is based on the measurement of PAR (400–700 nm) irradiance and spectral τ_a and obtains the best fit value of midvisible ω_0 from comparison of modeled cloudless sky PAR irradiance to measured values [*Eck et al.*, 1998, 2001; *Schafer et al.*, 2002a, 2002b]. The other method is similar but utilizes measurements of the spectral diffuse fraction measured by a seven channel MFRSR shadowband radiometer and spectral τ_a (from a CIMEL) to derive spectral ω_0 at five wavelengths from 415 to 870. These estimates are obtained by the best fit approach of comparing modeled to measured diffuse fraction and is similar to the method of ω_0 estimation described by *King and Herman* [1979].

5.1. ω_0 Retrieval From AERONET Almucantars

[29] All of the individual ω_0 retrievals from almucantar scans made at Zambezi, Zambia in August–September 2000 are shown in Figure 13. Additional cloud screening of cases where $\alpha_{440-870} < 1.7$ was applied to ensure that only biomass burning aerosol cases were analyzed and that

no cases with residual cloud contamination remained, although this additional check only eliminated 10 almucantars out of a total of 142. Figure 13 shows very little trend of ω_0 versus magnitude of τ_a, and linear regressions for all wavelengths yielded r^2 values of less than 0.07, thus explaining an insignificant amount of the variance. A similar lack of correlation was noted for ω_0 as a function of τ_a for the other five sites in Zambia in August–September 2000. In addition to the significant decrease in ω_0 as λ increases, the standard deviation of ω_0 also increases as λ increases, from 0.017 at λ = 440 nm to 0.032 at 1020 nm. This may possibly be related to greater variability in particle absorption properties for the larger sized particles but may also be a result of much lower τ_a at longer wavelengths, thus providing much less signal for aerosol optical property retrieval at the longer wavelengths.

[30] Comparisons of ω_0 retrieved from the application of the *Dubovik and King* [2000] algorithm to AERONET data against other techniques have recently been made. *Haywood et al.* [2003] compared their estimates of ω_0 obtained from in situ sampling with PMS probes from an aircraft that flew vertical profiles over the AERONET site at Etosha Pan, Namibia on 13 September 2000. A well-mixed biomass burning aerosol layer was present on this day with τ_{a440} = 0.71, as measured by the CIMEL. The comparison for this case yielded excellent agreement, with midvisible ω_0 values to within 0.01–0.02 of each other for the two completely independent techniques. For a different region of the world, *Ramanathan et al.* [2001] present a comparison of ω_0 estimates from several ground based in situ, aircraft in situ, and ground based remote sensing techniques made during the INDOEX experiment in 1999. For the polluted northern Indian Ocean region these methods estimated mean ω_0 at 530 nm to range from ∼0.85 to 0.90 for all total column-integrated and surface-based measurements, as compared to the AERONET estimate of 0.90. Therefore these independent methods also exhibited good agreement with the AERONET retrievals, mostly within the uncertainty of the
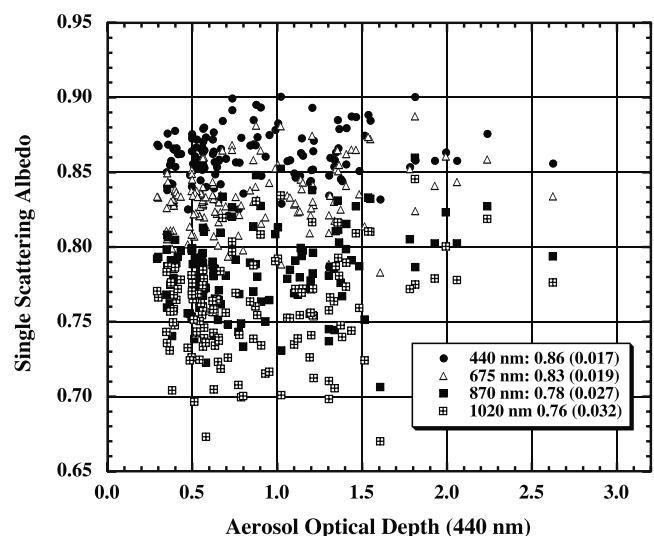

Figure 13. Individual almucantar scan retrievals of ω_0 in 4 spectral bands for Zambezi, Zambia for August–September 2000. The mean and standard deviation for each channel are shown in the legend box.
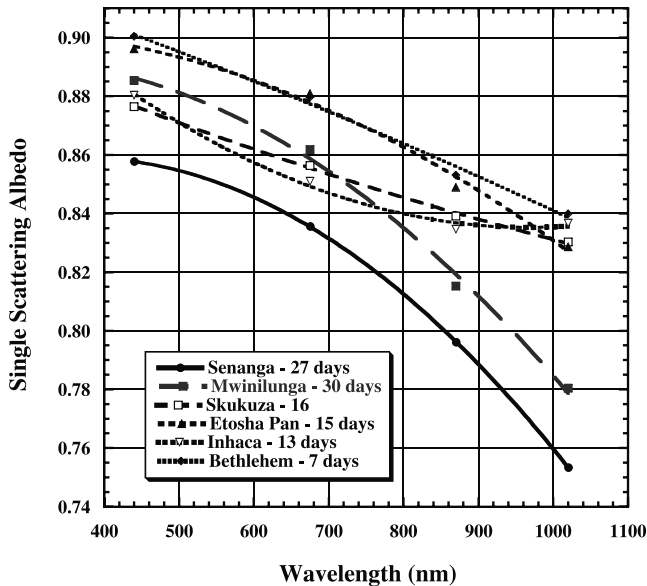
Figure 14. Regional scale variability of the average ω_0 for AERONET sites in southern Africa during August–September 2000 for retrievals made with $\tau_{a440} > 0.4$. From 7 to 30 daily mean ω_0 values were averaged per site in order to compute these values.

AERONET retrieval ($\sim$0.03 [*Dubovik et al.*, 2000]) and the uncertainties of the other retrieval methods.

[31] The regional scale variability of ω_0 over the AERONET sites in southern Africa during SAFARI 2000 is shown in Figure 14 and Table 1. The average spectral ω_0 for all cases where $\tau_{a440} > 0.4$ are compared, since there was no significant variation of ω_0 as a function of τ_a at any site. Daily average values of ω_0 were computed from individual almucantar retrieval values, and the mean of all of these daily averages are presented. The number of days averaged per site ranged from 30 days at Mwinilunga, Zambia, the northernmost site with the highest aerosol loadings, to 7 days at Bethlehem, South Africa, the southernmost site with the lowest aerosol concentrations. The two Zambian sites shown, Mwinilunga and Senanga, are the northernmost and southernmost sites respectively in Zambia and they show the widest range of retrieved ω_0 for Zambia (except Mongu which was excluded from this analysis since it did not have a consistent and accurate sky radiometer calibration). Although the ω_0 values at all wavelengths are higher at Mwinilunga than Senanga, these ω_0 differences are within the 0.03 level of uncertainty of the retrievals, however the difference may also reflect some real differences in absorption. The rate of spectral decrease of ω_0 is similar for both Zambian sites and also much greater than for the other four

sites which are located outside of the primary biomass burning regions. Also note that the mean spectral dependence of ω_0 at Zambezi (shown in Figure 13) is very similar to that of Senanga, within $\sim$0.01. The two sites with the least spectral dependence of ω_0 are Skukuza and Inhaca (Figure 14) which are only $\sim$200 km distant from each other. The size distributions for both of these sites show an enhanced coarse mode versus Senanga (Figure 12), and the average ω_0 at both of these sites was within 0.01 of each other at all wavelengths. The increased coarse mode influence at Skukuza and Inhaca results in a relatively greater scattering optical depth at the longer wavelengths (870 and 1020 nm) which results in a higher ω_0 value at these λ. The aerosol at both of these sites may include a component contribution of aeolian dust [*Piketh et al.*, 1999] and the ω_0 for dust generally exhibits little spectral dependence between 670 and 870 nm [*Dubovik et al.*, 2002]. The addition of aeolian dust mixed with biomass burning aerosols would thus tend to decrease the spectral dependence of ω_0, as was similarly observed for mixtures of fossil fuel and biomass combustion aerosol with dust in the Maldives in 2000 [*Eck et al.*, 2001]. The uncertainty of the single scattering albedo retrieval from the *Dubovik and King* [2000] algorithm for the case of an external mixture with refractive indices that are very different for each component (fine and coarse), remains at 0.03 [*Dubovik et al.*, 2000]. It is noted that aerosol contributions from fossil fuel burning and industrial emissions also influence the aerosol mixture at Skukuza and Inhaca, therefore also modifying the absorption characteristics. The spectral dependence of ω_0 for both Etosha Pan and Bethlehem are intermediate in magnitude to that of the Zambian site pair and the Skukuza/Inhaca pair. The ω_0 at both of these sites agree to within $\sim$0.01 and are higher than all of the others at the 440, 675 and 870 nm wavelengths. The size distribution at Etosha Pan (Figure 12) as compared to Senanga suggests a small increase in the coarse mode optical influence due to a greater coarse mode amplitude, shift toward smaller particles and larger geometric standard deviation. The higher ω_0 and lesser wavelength dependence at Etosha and Bethlehem may be the result of aerosol aging, as these sites (especially Bethlehem) are not located in the primary biomass burning regions to the north. Additionally, biomass burning aerosol often accumulate over the Atlantic Ocean west of Angola and Namibia (see Figure 7) and sometimes this smoke is then circulated back over Southern Africa, at times being advected over Etosha and Bethlehem. The resulting additional aging and a possible mixing with maritime aerosols may also affect the aerosol optical properties observed at these sites, along with the added possible influence of urban/industrial aerosols at Bethlehem. However, it is noted that the ω_0 data shown for Bethlehem in

Table 1. AERONET Retrievals of Aerosol Single Scattering Albedo (ω_0) for Cases Where $\tau_{a440} > 0.4$, for August–September 2000

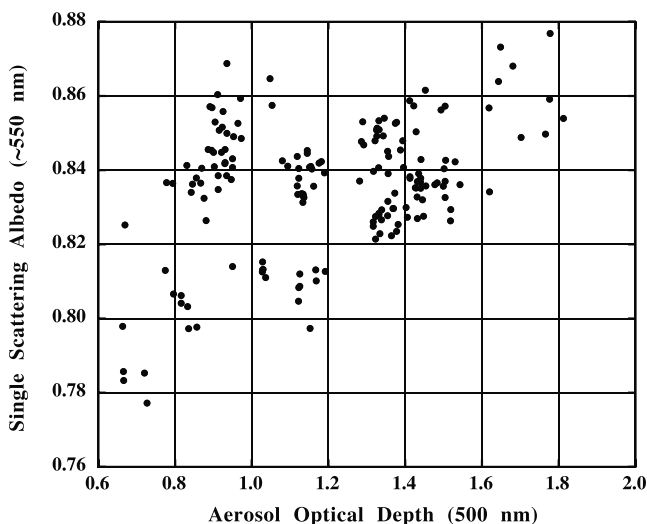| Wavelength, nm	Senanga, Zambia 27-Day Mean	Mwinilunga, Zambia 30-Day Mean	Skukuza, South Africa 16-Day Mean	Etosha Pan, Namibia 15-Day Mean	Inhaca Island, Mozambique 13-Day Mean	Bethlehem, South Africa 7-Day Mean
440	0.86	0.88	0.88	0.90	0.88	0.90
675	0.84	0.86	0.86	0.88	0.85	0.88
870	0.80	0.82	0.84	0.85	0.84	0.85
1020	0.75	0.78	0.83	0.83	0.84	0.84

Figure 15. Retrievals of midvisible ω_0 in Mongu, Zambia (August–September 2000) from best fitting of PAR (400–700 nm) flux measurements to modeled fluxes.

Figure 14 is based on only 7 days of data (only days where $\tau_{a440} > 0.4$) and therefore may be too small a sample to be considered representative.

5.2. ω_0 Retrieval From PAR Irradiance Data

[32] Aerosol single scattering albedo in the midvisible (~550 nm) was also estimated from the technique of fitting calculated to measured fluxes at the surface. This technique has been applied to PAR (400–700 nm) fluxes measured at Mongu, Zambia during the SAFARI 2000 campaign. The methodology and application of this technique has been described in detail elsewhere [*Eck et al.*, 1998, 2001; *Schafer et al.*, 2002a, 2002b] so only a brief description will be provided here. Solar flux attenuation by atmospheric aerosols is governed primarily by two parameters, spectral τ_a and ω_0 [*Lenoble*, 1991; *Eck et al.*, 1998; *Christopher et al.*, 2000]. We utilize the AERONET measured τ_a (uncertainty of 0.01–0.02) as input to the 6S model [*Vermote et al.*, 1997] to compute the cloudless sky fluxes. Aerosol refractive indices and aerosol volume size distribution are the other aerosol parameters utilized as input by the 6S model. The real part of the refractive index was assumed to be 1.53 and constant as function of wavelength. The volume size distribution is for smoke aerosol as determined from the *Dubovik and King* [2000] retrievals and is dynamic as a function of τ_a. The best fit value of the imaginary refractive index is then determined by matching modeled flux to measured flux. The 6S model utilizes Mie code computations in order to compute ω_0 from the complex refractive indices and the volume size distribution. This retrieval methodology was applied only to observations where $\tau_{a500} > 0.6$ in order to obtain sufficient sensitivity of fluxes to aerosol absorption. An additional constraint of solar zenith angle <45 degrees was applied in order to minimize the effects of sensor cosine response error. The uncertainty in these retrievals of ω_0 is estimated to be ~0.03 primarily due to uncertainty in flux instrument calibration, cosine response errors of the flux instrument, instrument leveling, assumed aerosol size distribution, assumed real part of the

refractive index, and uncertainty in the assumed surface albedo [*Eck et al.*, 1998, 2001]. The ω_0 values retrieved from this methodology for August–September 2000 ranged from 0.78 to 0.88 with a mean value of 0.84 (Figure 15). This mean value compares very well with the mean at 550 nm estimated from the AERONET measurements and *Dubovik and King* [2000] algorithm, by linear interpolation between the ω_0 at 440 and 675 nm. The estimated mean ω_0 at ~550 nm for four AERONET sites in Zambia (Senanga, Zambezi, Solwezi, and Ndola) for August–September is ~0.855, which is only ~0.015 greater than the PAR flux retrieval mean and well within the uncertainty of both retrieval techniques of ~0.03. Although there is a trend of increasing ω_0 as τ_{a500} increases (Figure 15), linear regression only explains ~15% of the variance, therefore this trend is not significant.

[33] A comparison of flux reductions in the PAR spectral region from biomass burning aerosols in Amazonia (Brazil) versus African savanna (Zambia) is shown in Figure 16. The ratio of measured fluxes to modeled background fluxes (background τ_{a500} is assumed to be 0.06) is shown as a function of τ_{a500} similar to the analyses of *Schafer et al.* [2002a, 2002b] for total shortwave fluxes. The attenuation of PAR fluxes at equivalent τ_{a500} is consistently greater for smoke in Zambian savanna as compared to that from a Brazilian tropical forest region. The retrieval of ω_0 from these PAR flux data average 0.91 for the Alta Floresta, Brazil site versus 0.84 for the Mongu, Zambia site. Differences in ω_0 at 550 nm of this magnitude ($\Delta\omega_0 = 0.07$) for the Amazonian forest smoke versus Zambian savanna smoke were also retrieved by the *Dubovik and King* [2000] algorithm from AERONET data [*Dubovik et al.*, 2002; *Eck et al.*, 2001]. These differences in ω_0 can be largely attributed to differences in the black carbon content of the aerosol that result from differences in the relative contribution of flaming versus smoldering combustion. Other factors that may contribute to differences in aerosol absorption between these two regions are differences in aerosol aging, fuel moisture content, fire intensity, and
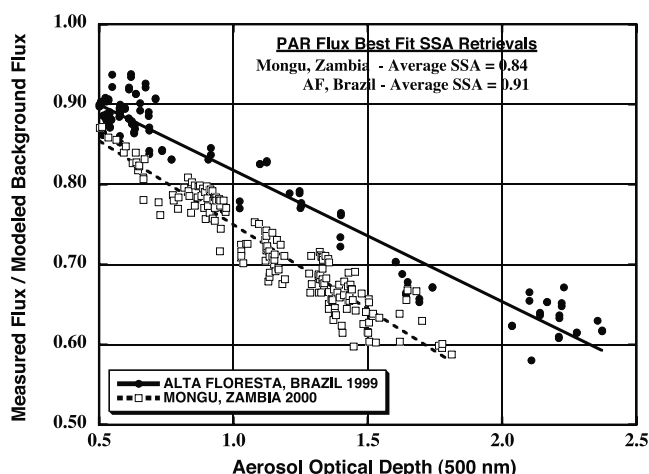

Figure 16. Comparison of relative PAR flux reductions (relative to background aerosol levels) as a function of biomass burning τ_{a500} for Mongu, Zambia in August–September 2000 versus Alta Floresta, Brazil (Amazonian forest region) in August–September 1999.
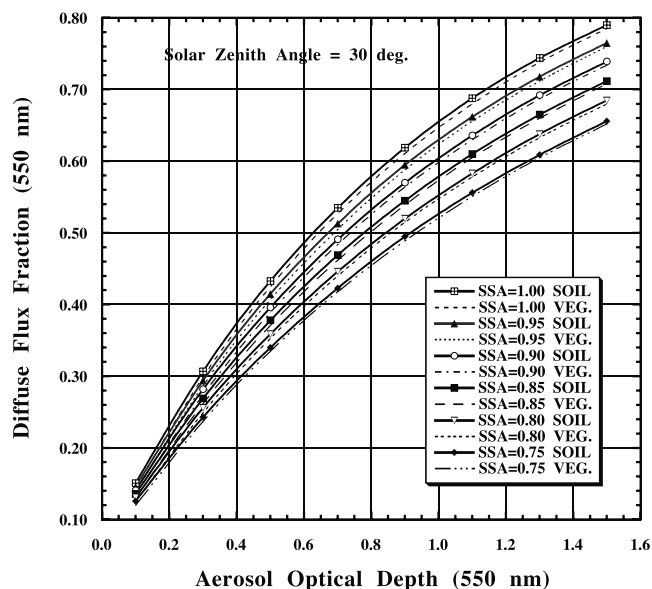
Figure 17. Diffuse fraction at 550 nm computed by the 6S model as a function of τ_{a550} for single scattering albedo (SSA) ranging from 0.75 to 1.0, solar zenith angle of 30°, and for surface reflectance representative of vegetation (0.06) and of soil (0.13).

cloud processing of aerosols. More detailed discussions of regional and continental differences in ω_0 for biomass burning aerosols are given by *Eck et al.* [2001] and *Dubovik et al.* [2002].

5.3. ω_0 Retrieval From Spectral Diffuse Fraction Measurements

[34] Spectral ω_0 values were also retrieved from measurements of the spectral diffuse fraction made with an MFRSR shadowband radiometer at Mongu, in conjunction with spectral τ_a data from the colocated AERONET radiometer. The methodology we utilize to retrieve the spectral imaginary refractive index, and the resulting computed ω_0, is similar in principal to the diffuse-direct ratio technique developed by *Herman et al.* [1975] and *King and Herman* [1979]. They showed that for a given value of ground albedo, the measured ratio of diffuse to direct solar flux is sensitive to the magnitude of the aerosol imaginary part of the refractive index. *King and Herman* [1979] also showed that there is relatively little sensitivity of the diffuse-direct ratio to the real part of the refractive index, and *Herman and Browning* [1975] showed that the vertical distribution of the atmospheric aerosols also has little influence on the diffuse flux at the Earth's surface. A distinct instrumental advantage of this technique over the measurement of absolute fluxes is that radiometer calibration is not required since the same detector is used to measure both flux components, which are then ratioed.

[35] Similar to the diffuse-direct ratio, we demonstrate that the ratio of diffuse flux to total flux (the diffuse fraction) is sensitive to aerosol absorption. In Figure 17 we show computations of the diffuse fraction at 550 nm from the 6S model for a solar zenith angle of 30°, for τ_{a550} ranging from 0.1 to 1.5 and aerosol single scattering albedo ranging from highly absorbing ($\omega_0 = 0.75$) to nonabsorbing

($\omega_0 = 1.0$). For these computations, the real part of the refractive index of 1.51 was assumed and the aerosol volume size distribution of biomass burning smoke in Zambian savanna [*Dubovik et al.*, 2002] was utilized. It is seen from Figure 17 that for moderate to high aerosol loadings ($\tau_{a550} = 0.5$ to 1.5) there is good sensitivity of the percent diffuse flux to the magnitude of ω_0. For example at $\tau_{a550} = 1.1$ a difference of ~0.03 in diffuse fraction corresponds to a 0.05 range in ω_0. Also shown in Figure 17 is the change in diffuse fraction which results from differences in Earth surface reflectance or albedo. The two surface albedo values compared were chosen to be representative of a vegetated surface (0.06 at 550 nm) and a sandy soil surface (0.13 at 550 nm). It is seen that at high τ_a there is relatively little influence on these changes in albedo
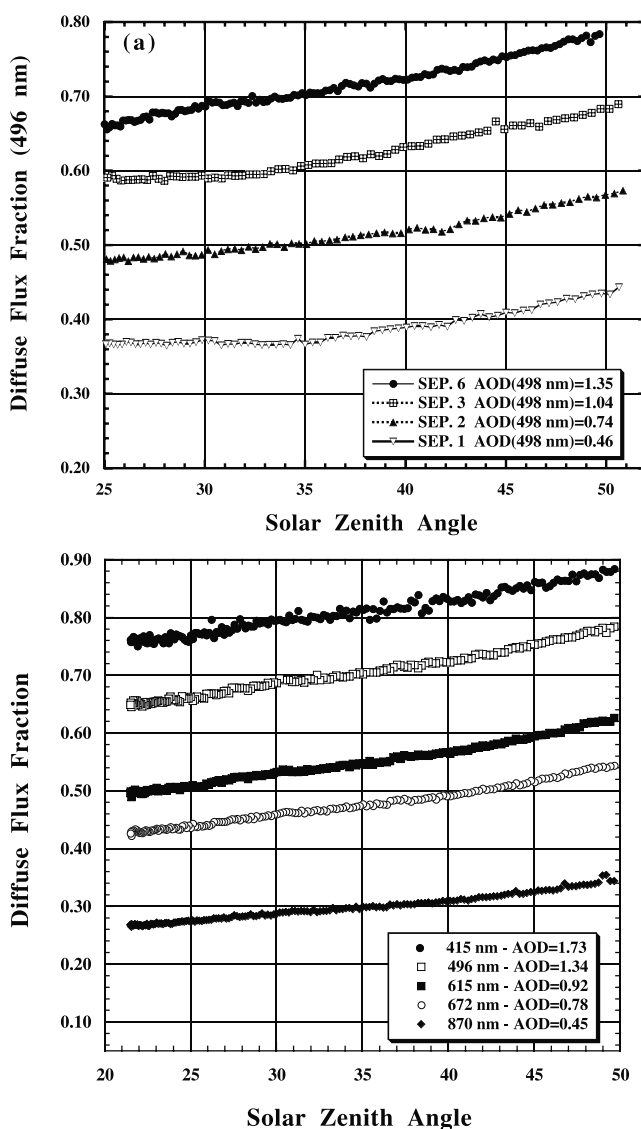

Figure 18. (a) Measurements of diffuse fraction at 496 nm made from an MFRSR radiometer in Mongu, Zambia during cloudless conditions on 4 days with differing τ_{a500} in September, 2000. (b) Spectral diffuse fraction measurements in Mongu on 6 September 2000 from 415 to 870 nm in 5 wavelengths with 10 nm bandpass.
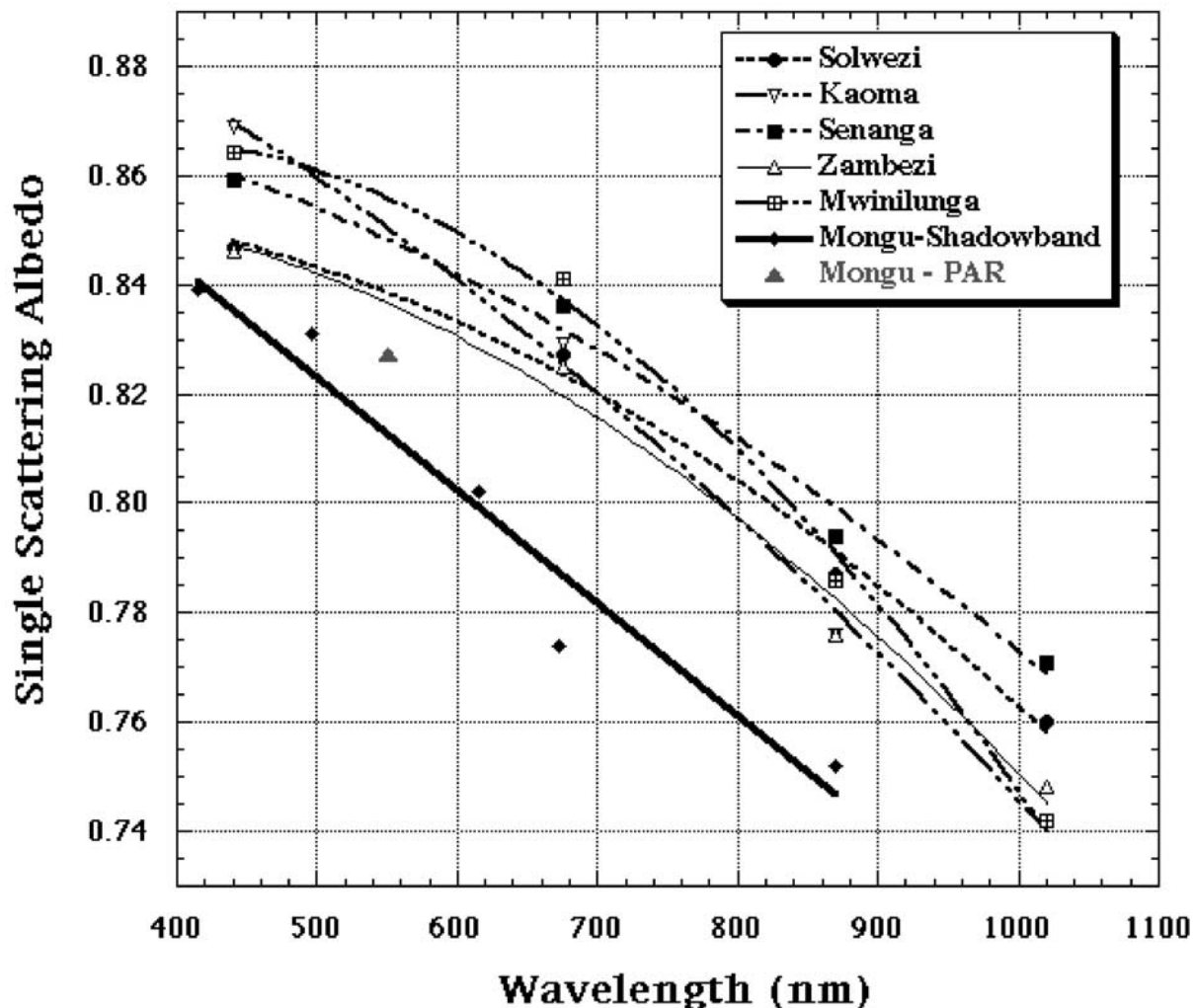
Figure 19. Spectral ω_o retrieval based on the diffuse fraction measurements (MSRFR shadowband) in Mongu on 6 September 2000 at 26° solar zenith angle (data shown in Figure 18b). Also shown are the spectral ω_o retrieved from AERONET almucantar scans for 5 other sites in western Zambia on the same date, and the midvisible ω_o at Mongu retrieved from PAR flux measurements. This day had heavy smoke aerosol loading ranging from $\tau_{a500} = 1.20$ to 2.01 at the 6 locations.

on the diffuse fraction. For example, at $\tau_{a550} = 1.1$ the difference in diffuse fraction due to this albedo difference is only $\sim$0.005 (six times less sensitivity than to a $\Delta\omega_0$ change of 0.05). However, at $\tau_{a550} = 0.3$ the diffuse fraction is about half as sensitive to this surface albedo change (Δalbedo = 0.07) as it is to an ω_0 change of 0.05. Therefore accurate retrieval of ω_0 from measurement of diffuse fraction at relatively low τ_a is only possible if there is accurate knowledge of both surface albedo and highly accurate measurement of diffuse fraction.

[36] Actual measurements of the spectral diffuse fraction at 496 nm taken with the MFRSR at Mongu, Zambia under cloudless conditions and varying τ_{a498} on 1, 2, 3, and 6 September 2000 are shown in Figure 18a. Large increases in diffuse fraction were observed as τ_{a498} increased from 0.46 on 1 September to 1.35 on 6 September 2000, as a result of both increasing direct beam solar attenuation and increasing diffuse irradiance from scattering by aerosols. Spectral variation in diffuse fraction is large due mainly to the large

spectral dependence of τ_a resulting from the dominance of fine mode particles in the biomass burning smoke and to a lesser extent from the spectral dependence of molecular (Rayleigh) optical depth which is highest at the shortest wavelengths. The spectral dependence of diffuse fraction is shown for 6 September 2000 at Mongu in Figure 18b where the average aerosol optical depth varies from 0.45 at 870 nm to 1.73 at 415 nm, corresponding to a diffuse fraction that is nearly three times greater at 415 than at 870 nm.

[37] An example of spectral ω_0 retrieval based on the measurement of the diffuse fraction is shown in Figure 19. This case is 6 September 2000 at 0932 UTC in Mongu when the CV-580 aircraft was flying an altitude profile over the CIMEL radiometer and MFRSR shadowband instruments [Sinha et al., 2003, Appendix] making extensive aerosol in situ measurements and vertical profiles of τ_a with the NASA Ames airborne Sun photometer [Schmid et al., 2003]. The biomass burning aerosol layer on this site and date was very stable with high aerosol optical depth.
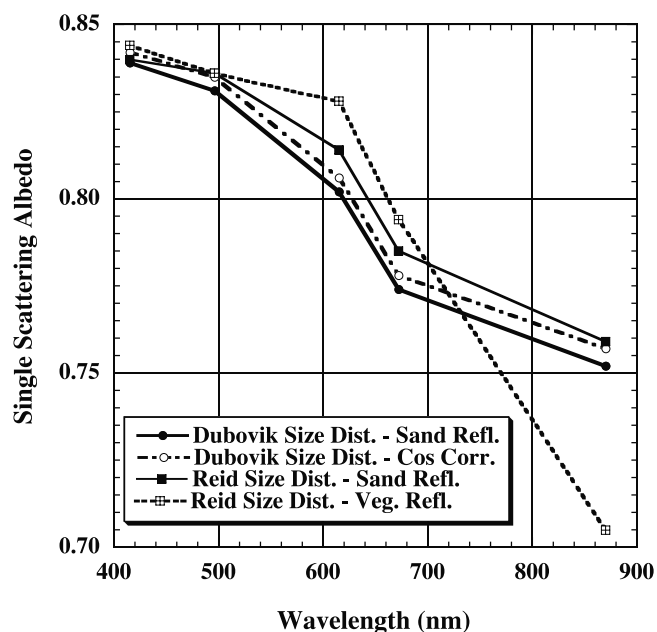
Figure 20. Diffuse fraction measurement-based retrievals of ω_o on 6 September 2000 in Mongu (same case as Figure 19) for different assumed aerosol size distributions, surface reflectance magnitude, and for cosine error correction applied to the diffuse fraction measurement.

For the four-hour period from 0700 to 1100 UTC the τ_{a498} averaged 1.34 with a standard deviation of only 0.013. The spectral τ_a ranged from 1.94 at 380 nm to 0.44 at 870 nm, therefore providing a high enough τ_a for the 415 to 870 nm range of the MFRSR in order to retrieve ω_0 from the diffuse fraction measurements (Figure 17). This retrieval of ω_0 from the diffuse fraction data was made at 26° solar zenith angle by fitting the computed diffuse fraction from the 6S model to the observed diffuse fraction, by varying the imaginary part of the refractive index. The real part of the refractive index was held spectrally constant at 1.51 and the aerosol size distribution of biomass burning aerosols in Zambia [*Eck et al.*, 2001] from the *Dubovik and King* [2000] algorithm retrievals was utilized. Retrievals of spectral ω_0 from the AERONET radiometers located at 5 sites in Zambia on this same day are also shown in Figure 19. These retrievals are for solar zenith angles greater than 50° ($\sim$ 2 hrs before the aircraft flight and the MFRSR data presented) in order to obtain sufficient scattering angle measurements of sky directional radiance to retrieve ω_0 with an accuracy of 0.03 [*Dubovik et al.*, 2000]. There is no ω_0 retrieval presented for the Mongu CIMEL due to a problem with the post deployment calibration of that instrument. This problem was avoided for the τ_a measurements since the CIMEL instrument is composed of two independent radiometers (one for direct Sun and the other for sky radiance) and the direct Sun calibration was accurately determined by inter-calibration with freshly calibrated CIMELs brought to Mongu in August 2000 during the SAFARI experiment.

[38] The differences between the ω_0 retrievals from the five AERONET CIMELs in western Zambia on this date are relatively small with a range of $\sim$0.02–0.03 depending on

wavelength (Figure 19). Part of these differences may be due to physical differences in the aerosol at the various sites and part may also be due to instrumental/calibration differences. The spectral dependence of the ω_0 values retrieved from the diffuse fraction technique exhibit a very similar slope to the ω_0 from the AERONET retrievals. The absorption Angstrom exponent (α_{abs}) for Mongu on 6 September 2000 was computed from the absorption optical depths

$$\tau_{abs}\lambda = \tau_a\lambda \cdot (1 - \omega_0\lambda) \qquad (1)$$

over the 415 to 870 nm wavelength interval. A linear fit of ln $\tau_{abs\lambda}$ versus ln λ was used to compute α_{abs}, which equals 1.34 if ω_0 from the Senanga AERONET retrievals were used and 1.19 if the MFRSR shadowband retrievals of ω_0 were utilized. This compares to an Angstrom exponent of 1.88 computed from a linear fit of the spectral total aerosol optical depth (τ_a) at 440, 675, and 870 nm. Although the slope of ω_0 with wavelength is quite similar for the two retrieval methods, the values of ω_0 from the diffuse fraction method are $\sim$0.02–0.04 lower than the mean of the *Dubovik and King* [2000] retrievals (Figure 19). It is noted that the ω_0 retrieval from fitting the modeled to measured PAR fluxes averaged $\sim$0.826 on 6 September 2000 which is $\sim$0.015 higher than the diffuse fraction retrieval interpolated to 550 nm. Comparisons of shadowband versus AERONET ω_0 retrievals on two other dates (2 and 3 September 2000) in Mongu, yielded very similar differences with lower values from the shadowband retrievals.

[39] The principal sources of uncertainty in computing ω_0 from the diffuse fraction technique are cosine response error of the MFRSR detector, instrument leveling error, an error associated with blocking sky radiance when shading the Sun, an error in assumed size distribution when computing cloudless flux, and an error in the assumed magnitude of the surface spectral albedo. Yankee Environmental Systems, Inc. provides the measured (to zenith) cosine response for each MFRSR channel and these values were used to estimate the error in diffuse fraction that results from this nonideal cosine response. The direct radiation component which is computed as the difference between the Sun blocked (shaded) and unshaded radiometer is corrected for cosine response error, but the diffuse component is not. Utilizing the measurements of cosine response error (given at 1° intervals from 1 to 90°) we computed an underestimation of $\sim$1% in the diffuse flux component. This error in diffuse flux results in an error in diffuse fraction that reaches a maximum of 0.005 at 0.50 diffuse fraction and zero error at 0.0 and 1.0 diffuse fraction. In Figure 20 we show the magnitude of the estimated cosine response error on the retrieval of ω_0 for the same case as is shown in Figure 19. An error in leveling of the instrument will also result in maximum errors at a diffuse fraction of 0.50, with the errors in direct irradiance being larger than for diffuse irradiance. For example, simulations with the SPCTRAL2 model [*Bird and Riordan*, 1986] for the case shown in Figure 19, show that a 2° error in leveling at 26° solar zenith angle will result in a 0.003 error in diffuse fraction at 415 nm where the diffuse fraction is 0.773 and also a 0.003 error at 870 nm where the diffuse fraction is 0.277, and a maximum error in diffuse fraction of 0.004 when the diffuse fraction
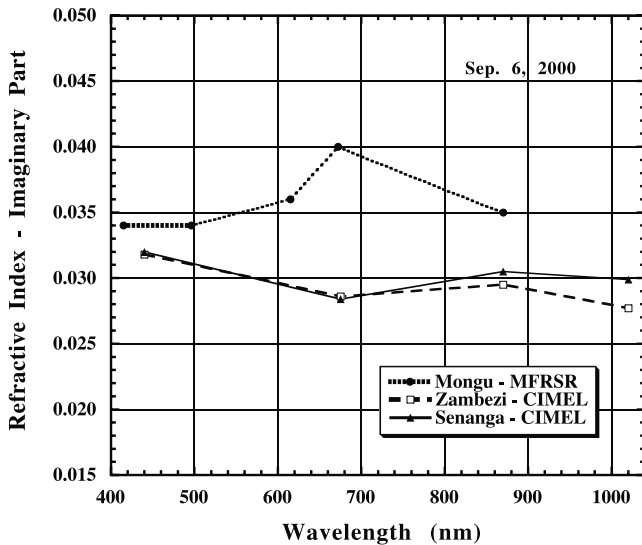
Figure 21. The wavelength dependence of the imaginary part of the refractive index retrieved from the diffuse fraction measurement method at Mongu and from the AERONET retrievals for the sites immediately to the north and south of Mongu, all on 6 September 2000.

is ~0.50. The portion of sky radiance blocked when shading the direct Sun is compensated for by adding a diffuse flux measurement representative of the blocking band area at 9° from the Sun [*Harrison et al.*, 1994], since the shadowband measures the diffuse flux at 9° to the side of the Sun both before and after shading the Sun. Figure 20 also shows the effect of varying the assumed aerosol size distribution on the retrieval of ω_0. The size distribution for Cuiaba local smoke [*Reid et al.*, 1998] was utilized since this is smoke from a South American cerrado region which is somewhat similar to savanna woodland in southern Africa. The difference in the retrieval utilizing AERONET size distributions versus the Reid et al. distribution is nearly zero at 415 nm and ~0.01 at wavelengths greater than 600 nm. The larger errors at longer wavelengths result partly from a lack of any coarse mode in the Reid et al. size distribution, thus resulting in a more strongly backscattering aerosol which then yields a higher retrieval value of ω_0, since some additional attenuation is caused by backscatter rather than absorption. The influence of the assumed value of spectral ground albedo is also show in Figure 20. The two extremes are shown, where spectral reflectance representative of bare soil is compared to that of a 100% green vegetated surface. Again the differences in retrieval at 415 nm are very small, since the reflectance of both surface types at this wavelength are nearly equal and relatively low. However, at wavelengths greater than 600 nm, significant differences in ω_0 retrieval result due to large differences in assumed surface reflectance (at 870 nm the soil reflectance in the 6S model is 0.292 while for vegetation it is 0.531). We have no measurements of the actual surface reflectance at the Mongu airport site where the MFRSR measurements were taken, but approximately 90% or less of surface had green vegetation, with the surface covered mainly by senescent brown grass or sandy soil in September, which

is near the end of the severe dry season. Therefore the actual surface reflectance should be much closer to the assumed sandy soil reflectance values than to a completely vegetated surface.

[40] All sources of measurement error (cosine error, leveling, diffuse sky blockage) combined result in an error in the diffuse fraction that is maximum at a diffuse fraction of 0.50, where we estimate the total uncertainty to be ~0.01. At diffuse fraction levels of 0.75 and 0.25, the measurement uncertainty results in a lower error, ~0.005 in diffuse fraction. Thus for the case of 6 September 2000 (26° solar zenith) presented in Figure 19, the maximum error due to measurement uncertainty will occur for the 615 and 672 nm data where diffuse fraction is 0.51 and 0.44 respectively. The uncertainty in ω_0 retrieval due to these measurement errors are ~0.02. The uncertainty in retrieval due to assumptions about the aerosol size distribution and the surface reflectance are both much larger for wavelengths greater than 600 nm (Figure 20). Therefore the close agreement between the AERONET and diffuse fraction measurement based retrieval of ω_0 at 415 and 498 nm (differences of ~0.01–0.02; Figure 19) is most likely due in part to a higher τ_a at shorter wavelengths (greater absorption signal), relatively low uncertainty in both key assumptions (aerosol size distribution and spectral surface reflectance), and also low measurement errors of the diffuse fraction. At wavelengths greater than 600 nm, the difference in retrieved ω_0 of ~0.04 between these two methods may possibly be explained by a combination of both the AERONET retrieval uncertainty of ~0.03 and the greater uncertainties in the ω_0 retrievals from diffuse fraction data due to combined measurement and assumption uncertainties (Figure 20).

[41] The wavelength dependence of the imaginary part of the refractive index (k) as retrieved from the AERONET data and the *Dubovik and King* [2000] algorithm and from the diffuse fraction fitting retrieval from the MFRSR data, is shown in Figure 21. The MFRSR data-based retrieval at Mongu is compared to the CIMEL data-based retrieval for the AERONET sites closest to the north and south of Mongu (Zambezi and Senanga) for 6 September 2000, the same case as shown in Figure 19. Both methods retrieved relatively constant spectral values of the imaginary index (with the exception of 670 nm for the MFRSR). This spectral dependence is in good agreement with the data and analysis presented by *Bergstrom et al.* [2002], who suggest that black carbon (soot) exhibits relatively little wavelength dependence of k in the 400 to 1000 nm range and that this results in a decrease in single scattering albedo as wavelength increases for fine mode aerosols that are mixtures of black carbon and nonabsorbing material.

6. Summary and Conclusions

[42] A regional network of several AERONET Sun-sky radiometers was established in southern Africa for the SAFARI 2000 dry season campaign in August–September 2000, to augment the AERONET long-term monitoring sites in the region. Data from 10 primary sites in this network were utilized to investigate the spatial, temporal, and spectral variance of the total column-integrated radia-

tively effective aerosol optical properties in the region. The aerosol at many of these sites is dominated by biomass burning aerosols in this period, however aeolian dust, fossil fuel combustion aerosols, and maritime aerosols also contribute to the mixture at some sites, especially in the south (South Africa and Mozambique). The principal findings of our study are summarized as follows:

1. Long-term monitoring (7 years) in Mongu, Zambia of biomass burning aerosols shows that the August 2000 monthly mean aerosol optical depth was lower than normal (τ_{a500} = 0.31 versus 0.39 for the multiyear mean), while the September 2000 aerosol optical depth was much higher than the mean September value (τ_{a500}=0.86 versus a mean of 0.65). This very large increase of aerosol optical depth between these two months in 2000 resulted largely from significant shifts in regional circulation [*Swap et al.*, 2002; Stein et al., submitted manuscript, 2002].

2. Within Zambia a clear North-South gradient in τ_a was observed in August, while in September there is a lack of such a gradient, as episodes of large scale transport of air with high smoke concentrations dominate. However, over the larger regional scale throughout southern Africa (sites in Zambia (ZAM), Namibia (NAM), South Africa (RSA), and Mozambique (MOZ)) in September, there was a large north-south gradient due to the location of major biomass burning regions in the north and the dispersion and deposition of smoke as it was advected southward. The Angstrom exponent ($\alpha_{440-870}$) also exhibited significant regional variability with the lowest values at Inhaca Island, MOZ (possible influences of sea salt, aeolian dust, and coarse mode industrial particles) and highest at Mongu, ZAM where fine mode biomass burning aerosols dominate. The size distribution retrievals at both Skukuza, RSA and Inhaca Island, MOZ showed significantly greater coarse mode contributions than the biomass burning dominated size distributions in Mongu, ZAM and Etosha Pan, NAM.

3. Significant average diurnal trends of τ_a were observed for all six sites in Zambia, with a typical minimum to maximum range of ~25% (August–September average), with the minimum occurring one hour before local noon and a maximum at sunset. This is related to the diurnal trends in fire count number which peak at ~3 hours after noon in this active burning region. In contrast, there was little or no significant average diurnal τ_a trend observed for sites located to the south of Zambia, since aerosol advection by winds is dominant at these sites, and this has more random temporal variation.

4. The ω_o inferred from AERONET retrievals at all of the Zambian sites showed no significant trend as a function of τ_a for the range of τ_{a440} from 0.4 to 2.5. The wavelength dependence of ω_o was very similar for all the sites in Zambia, however ω_o spectral variability was much greater on the regional scale throughout southern Africa. Although the ω_o at 440 and 675 nm for Skukuza, RSA and Inhaca, MOZ were very similar to values in Zambia, the ω_o at 870 and 1020 nm were significantly higher than in Zambia (~0.06 higher at 1020 nm). These differences are partly the result of greater coarse mode aerosol contributions at Skukuza and Inhaca (possibly from aeolian dust), which results in relatively greater scattering optical depths in the longer near-infrared wavelengths. Other factors are the differences in aerosol types, with fossil fuel combustion and

industrial emissions affecting the South African and Mozambique sites in addition to the biomass burning aerosols.

5. Single scattering albedo retrieved from the fitting of PAR flux measurements to modeled fluxes yielded a September–August 2000 average midvisible ω_o in Mongu, Zambia of 0.84. This is similar to the average midvisible estimates from the 440 and 675 nm AERONET retrievals of ~0.85, well within the uncertainties of the retrievals for both methods.

6. Spectral ω_o was also independently retrieved from diffuse fraction measurements at Mongu and the slope of the spectral dependence of ω_o (415–870 nm) from these retrievals is similar to those from the AERONET retrievals, with ω_o from diffuse fraction retrievals being ~0.02–0.04 lower (greater differences at longer wavelengths, possibly due to combined measurement error and model assumptions). Retrievals of the imaginary part of the refractive index show relatively constant values as a function of wavelength for both AERONET and diffuse fraction techniques.

[43] Therefore although the biomass burning aerosol optical properties measured at several sites in Zambia during August–September 2000 were relatively uniform, over the broader region the observations suggest significant aerosol variability. The observed regional differences in aerosol single scattering albedo and size distributions, due to aerosol aging during transport and from contributions by other aerosol sources (i.e. aeolian dust, fossil fuel combustion aerosols, etc.), need to be considered when assessing regional aerosol radiative forcings and retrieval of aerosol properties from satellite. Aerosol optical properties may also change seasonally in southern Africa and this aspect of regional aerosol dynamics is being examined in another study.

References

Ackerman, A. S., O. B. Toon, D. E. Stevens, A. J. Heymsfield, V. Ramanathan, and E. J. Welton, Reduction of tropical cloudiness by soot, *Science*, 288, 1042–1047, 2000.

Annegarn, H. J., L. Otter, R. J. Swap, and R. J. Scholes, Southern Africa's ecosystem in a test-tube–A perspective on the Southern African Regional Science Initiative (SAFARI 2000), *S. Afr. J. Sci.*, 98, 111–113, 2002.

Bergstrom, R. W., P. B. Russell, and P. Hignett, Wavelength dependence of the absorption of black carbon particles: Predictions and results from the TARFOX experiment and implications for the aerosol single scattering albedo, *J. Atmos. Sci.*, 59, 567–575, 2002.

Bird, R. E., and C. Riordan, Simple solar spectral model for direct and diffuse irradiance on horizontal and tilted planes at the Earth's surface for cloudless atmospheres, *J. Clim. Appl. Meteorol.*, 25, 87–97, 1986.

Campbell, J. R., E. Welton, J. D. Spinhirne, Q. Ji, S-C. Tsay, S. J. Piketh, M. Barenbrug, and B. N. Holben, Lidar observations of tropospheric aerosols over northeastern South Africa during the ARREX and SAFARI-2000 dry season experiments, *J. Geophys. Res.*, this issue.

Christopher, S. A., X. Li, R. M. Welch, J. S. Reid, P. V. Hobbs, T. F. Eck, and B. N. Holben, Estimation of surface and top-of-atmosphere shortwave irradiance in biomass burning regions during SCAR-B, *J. Appl. Meteorol.*, 39, 1742–1753, 2000.

Dubovik, O., and M. D. King, A flexible inversion algorithm for the retrieval of aerosol optical properties from Sun and sky radiance measurements, *J. Geophys. Res.*, *105*, 20,673–20,696, 2000.

Dubovik, O., A. Smirnov, B. N. Holben, M. D. King, Y. J. Kaufman, T. F. Eck, and I. Slutsker, Accuracy assesments of aerosol optical properties retrieved from AERONET Sun and sky-radiance measurements, *J. Geophys. Res.*, *105*, 9791–9806, 2000.

Dubovik, O., B. N. Holben, T. F. Eck, A. Smirnov, Y. J. Kaufman, M. D. King, D. Tanre, and I. Slutsker, Climatology of atmospheric aerosol absorption and optical properties in key locations, *J. Atmos. Sci.*, *59*, 590–608, 2002.

Dwyer, E., J.-M. Gregoire, and J.-P. Malingreau, A global analysis of vegetation fires using satellite images: Spatial and temporal dynamics, *Ambio*, *27*, 175–181, 1998.

Eck, T. F., B. N. Holben, I. Slutsker, and A. Setzer, Measurements of irradiance attenuation and estimation of aerosol single scattering albedo for biomass burning aerosols in Amazonia, *J. Geophys. Res.*, *103*, 31,865–31,878, 1998.

Eck, T. F., B. N. Holben, J. S. Reid, O. Dubovik, A. Smirnov, N. T. O'Neill, I. Slutsker, and S. Kinne, Wavelength dependence of the optical depth of biomass burning, urban, and desert dust aerosols, *J. Geophys. Res.*, *104*, 31,333–31,349, 1999.

Eck, T. F., B. N. Holben, D. E. Ward, O. Dubovik, J. S. Reid, A. Smirnov, M. M. Mukelabai, N. C. Hsu, N. T. O'Neill, and I. Slutsker, Characterization of the optical properties of biomass burning aerosols in Zambia during the 1997 ZIBBEE Field Campaign, *Geophys. Res.*, *106*, 3425–3448, 2001.

Garstang, M., P. D. Tyson, R. Swap, M. Edwards, P. Kallberg, and J. A. Lindesay, Horizontal and vertical transport of air over southern Africa, *J. Geophys. Res.*, *101*, 23,721–23,736, 1996.

Hansen, J., M. Sato, and R. Ruedy, Radiative forcing and climate response, *J. Geophys. Res.*, *102*, 6831–6864, 1997.

Hansen, J., M. Sato, R. Ruedy, A. Lacis, and V. Oinas, Global warming in the twenty-first century: An alternative scenario, *Proc. Natl. Acad. Sci. U. S. A.*, *97*, 9875–9880, 2000.

Harrison, L., J. Michalsky, and J. Berndt, Automated multifilter rotating shadow-band radiometer—An instrument for optical depth and radiation measurements, *Appl. Opt.*, *33*, 5118–5125, 1994.

Haywood, J. M., and V. Ramaswamy, Global sensitivity studies of the direct radiative forcing due to anthropogenic sulfate and black carbon aerosols, *J. Geophys. Res.*, *103*, 6043–6058, 1998.

Haywood, J. M., P. Francis, O. Dubovik, M. Glew, and B. N. Holben, Comparisons of aerosol size distributions, radiative properties and optical depths determined by aircraft observations and sunphotometers during SAFARI-2000, *J. Geophys. Res.*, *108*, doi:10.1029/2002JD002250, in press, 2003.

Herman, B. M., and R. S. Browning, Effect of aerosols on earth-atmosphere albedo, *J. Atmos. Sci.*, *32*, 1430–1445, 1975.

Herman, B. M., R. S. Browning, and J. J. Deluisi, Determination of effective imaginary term of complex refractive-index of atmospheric dust by remote-sensing—Diffuse-direct radiation method, *J. Atmos. Sci.*, *32*, 918–925, 1975.

Holben, B. N., et al., AERONET—A federated instrument network and data archive for aerosol characterization, *Remote Sens. Environ.*, *66*, 1–16, 1998.

Holben, B. N., et al., An emerging ground-based aerosol climatology: Aerosol Optical Depth from AERONET, *J. Geophys. Res.*, *106*, 12,067–12,097, 2001.

Houghton, J. T., et al., (Eds.), *Climate Change, 2001: The Scientific Basis*, 896 pp., Cambridge Univ. Press, New York, 2001.

Hsu, N. C., J. R. Herman, O. Torres, B. N. Holben, D. Tanre, T. F. Eck, A. Smirnov, B. Chatenet, and F. Lavenu, Comparisons of the TOMS aerosol index with sunphotometer aerosol optical thickness: Results and applications, *J. Geophys. Res.*, *104*, 6269–6279, 1999.

Jacobson, M. Z., Strong radiative heating due to the mixing state of black carbon in atmospheric aerosols, *Nature*, *409*, 695–697, 2001.

Justice, C. O., J. D. Kendall, P. R. Dowtry, and R. J. Scholes, Satellite remote sensing of fires during the SAFARI campaign using NOAA advanced very high resolution radiometer data, *J. Geophys. Res.*, *101*, 23,851–23,863, 1996.

Kaufman, Y. J., B. N. Holben, D. Tanré, I. Slutsker, A. Smirnov, and T. F. Eck, Will aerosol measurements from Terra and Aqua polar orbiting satellites represent the daily aerosol abundance and properties?, *Geophys. Res. Lett.*, *27*, 3861–3864, 2000.

King, M. D., and B. M. Herman, Determination of the ground albedo and the index of absorption of atmospheric particulates by remote-sensing, 1, Theory, *J. Atmos. Sci.*, *36*, 163–173, 1979.

Kinne, S., T. P. Ackerman, M. Shiobara, A. Uchiyama, A. J. Heymsfield, L. Miloshevich, J. Wendell, E. W. Eloranta, C. Purgold, and R. W. Bergstrom, Cirrus cloud radiative and microphysical properties from ground observations and in situ measurements during FIRE 1991 and their application to exhibit problems in cirrus solar radiative transfer modeling, *J. Atmos. Sci.*, *54*, 2320–2344, 1997.

Lenoble, J., The particulate matter from biomass burning: A tutorial and critical review of its radiative impact, in *Global Biomass Burning: Atmospheric, Climatic, and Biospheric Implications*, chap. 46, edited by J. S. Levine, pp. 381–386, MIT Press, Cambridge, Mass., 1991.

Magi, B., and P. V. Hobbs, Effects of humidity on aerosols in southern Africa during the biomass burning season, *J. Geophys. Res.*, *108*, doi:10.1029/2002JD002144, in press, 2003.

Martins, J. V., P. V. Hobbs, R. E. Weiss, and P. Artaxo, Sphericity and morphology of smoke particles from biomass burning in Brazil, *J. Geophys. Res.*, *103*, 32,051–32,057, 1998.

O'Neill, N. T., T. F. Eck, B. N. Holben, A. Smirnov, O. Dubovik, and A. Royer, Bimodal size distribution influences on the variation of Angstrom derivatives in spectral and optical depth space, *J. Geophys. Res.*, *106*, 9787–9806, 2001.

Piketh, S. J., H. J. Annegarn, and P. D. Tyson, Lower tropospheric aerosol loadings over South Africa: The relative contribution of aeolian dust, industrial emissions, and biomass burning, *J. Geophys. Res.*, *104*, 1597–1607, 1999.

Prins, E. M., J. M. Feltz, W. P. Menzel, and D. E. Ward, An overview of GOES-8 diurnal fire and smoke results for SCAR-B and 1995 fire season in South America, *J. Geophys. Res.*, *103*, 31,821–31,835, 1998.

Queface, A. S., J. Piketh, H. Annegarn, B. Holben, and R. Uthui, Retrieval of aerosol optical thickness and size distribution from Cimel sun photometer over Inhaca Island, Mozambique, *J. Geophys. Res.*, this issue.

Ramanathan, V., et al., The Indian Ocean Experiment: An integrated analysis of the climate forcing and effects of the great Indo-Asian haze, *J. Geophys. Res.*, *106*, 28,371–28,398, 2001.

Reid, J. S., P. V. Hobbs, R. J. Ferek, D. R. Blake, J. V. Martrins, M. R. Dunlap, and C. Liousse, Physical, chemical, and optical properties of regional hazes dominated by smoke in Brazil, *J. Geophys. Res.*, *103*, 32,059–32,080, 1998.

Reid, J. S., T. F. Eck, S. A. Christopher, P. V. Hobbs, and B. N. Holben, Use of the Angstrom exponent to estimate the variability of optical and physical properties of aging smoke particles in Brazil, *J. Geophys. Res.*, *104*, 27,473–27,489, 1999.

Schafer, J. S., B. N. Holben, T. F. Eck, M. A. Yamasoe, and P. Artaxo, Atmospheric effects on insolation in the Brazilian Amazon: Observed modification of solar radiation by clouds and smoke and derived single scattering albedo of fire aerosols, *J. Geophys. Res.*, *107*, 8074, 10.1029/2001JD000428, 2002a.

Schafer, J. S., T. F. Eck, B. N. Holben, P. Artaxo, M. A. Yamasoe, and A. S. Procopio, Observed reductions of total solar irradiance by biomass-burning aerosols in the Brazilian Amazon and Zambian Savanna, *Geophys. Res. Lett.*, *20*, 1823, doi:10.1029/2001GL014309, 2002b.

Schmid, B., J. Michalsky, R. Halthore, M. Beauharnois, L. Harrison, J. Livingston, P. Russell, B. Holben, T. Eck, and A. Smirnov, Comparison of aerosol optical depth from four solar radiometers during the Fall 1997 ARM intensive observation period, *Geophys. Res. Lett.*, *26*, 2725–2728, 1999.

Schmid, B., et al., Coordinated airborne, spaceborne, and ground-based measurements of massive, thick aerosol layers during dry season in Southern Africa, *J. Geophys. Res.*, *108*, doi:10.1029/2002JD002297, in press, 2003.

Scholes, C. O., J. D. Kendall, and C. O. Justice, The quantity of biomass burned in southern Africa, *J. Geophys. Res.*, *101*, 23,667–23,676, 1996.

Sinha, P., P. V. Hobbs, R. J. Yokelson, I. Bertschi, D. R. Blake, I. J. Simpson, S. Gao, T. L. Kirchstetter, and T. Novakov, Emissions of trace gases and particles from savanna fires in southern Africa, *J. Geophys. Res.*, *108*, doi:10.1029/2002JD002325, in press, 2003.

Smirnov, A., B. N. Holben, T. F. Eck, O. Dubovik, and I. Slutsker, Cloud screening and quality control algorithms for the AERONET data base, *Remote Sens. Environ.*, *73*, 337–349, 2000.

Swap, R. J., et al., The Southern African Regional Science Initiative (SAFARI 2000): Overview of the dry season field campaign, *S. Afr. J. Sci.*, *98*, 125–130, 2002.

Torres, O., P. K. Bhartia, J. R. Herman, Z. Ahmad, and J. Gleason, Derivation of aerosol properties from satellite measurements of backscattered ultraviolet radiation: Theoretical basis, *J. Geophys. Res.*, *103*, 17,099–17,110, 1998.

Vermote, E. F., D. Tanre, J. L. Deuze, M. Herman, and J. J. Morcrette, Second Simulation of the Satellite Signal in the Solar Spectrum, 6S: An overview, *IEEE Trans. Geosci. Remote Sens.*, *35*, 675–686, 1997.

Ward, D. E., R. A. Susott, J. B. Kaufman, R. E. Babbitt, D. L. Cummings, B. Dias, B. N. Holben, Y. J. Kaufman, R. A. Rasmussen, and A. W. Setzer, Smoke and fire characteristics for cerrado and deforestation burns in Brazil: Base-B experiment, *J. Geophys. Res.*, *97*, 14,601–14,619, 1992.

Ward, D. E., W. M. Hao, R. A. Susott, R. E. Babbitt, R. W. Shea, J. B. Kaufman, and C. O. Justice, Effect of fuel composition on combustion efficiency and emission factors for African savanna ecosystems, *J. Geophys. Res.*, *101*, 23,569–23,576, 1996.

———————————

O. Dubovik, T. F. Eck, N. C. Hsu, and A. Smirnov, Goddard Earth Sciences and Technology Center, University of Maryland-Baltimore County, Baltimore, MD, USA. (tom@aeronet.gsfc.nasa.gov)

B. N. Holben, J. S. Schafer, and I. Slutsker, Biospheric Sciences Branch, Code 923, NASA/Goddard Space Flight Center, Greenbelt, MD, USA.

J. Le Roux, Etosha Ecological Institute, Okaukuejo, Namibia.

M. M. Mukelabai, Zambian Meteorological Department, Mongu, Zambia.

S. J. Piketh and A. Queface, Climatology Research Group, University of Witwatersrand, Gauteng, South Africa.

R. J. Swap, Department of Environmental Sciences, University of Virginia, Charlottesville, VA, USA.

D. E. Ward, Enviropyronics, White Salmon, WA, USA.